

Supporting Information

PM-IRRAS and DFT investigation of the surface orientation of new Ir piano-stool complexes attached to Au (111)

*Christopher J. Miller, Felix M. Brunner, H. Ray Kelly, Po Ling Cheung, Nicole A. Torquato,
Milan Gembicky, Saya Okuno, Thomas Chan, Victor S. Batista, Clifford P. Kubiak**

Department of Chemistry and Biochemistry, University of California, San Diego, 9500 Gilman Drive, Mail Code 0358, La Jolla, California 92093-0358

Department of Chemistry and Energy Sciences Institute, Yale University, 225 Prospect Street, New Haven, Connecticut 06520, United States

Table of Contents

Contents

Experimental Methods	2
Simulated isotropic IRRAS spectra.....	2
Comparison of the PM-IRRAS and the Simulated IRRAS via Spectral Fitting.....	3
Determination of Surface Coverage by ICP-MS.....	3
Characterization of SAMs by X-ray photoelectron spectroscopy (XPS).....	3
NMR Spectra	4
IR-Spectra	10
FTIR Spectra of KBr Pellets	15
Molar Absorptivity and Refractive Index	16
Mass Spectra	17
ICP-MS determination of surface coverage.....	21
Parameters for IRRAS Simulation.....	21
Raw PM-IRRAS	22
PM-IRRAS and Simulated IRRAS with Fits.....	23
PM-IRRAS Peak Fitting Analysis	25
Computational Benchmarking	28

Comparison of the Experimental and DFT calculated TDMs for orientation determination. ..	28
DFT Computed FTIR.....	29
DFT Optimized Structure Parameters.....	31
Relative Intensity and Transition Dipole Analysis with Computed Orientations.....	32
TDM analysis using Functional: PBE D3 Basis Set: LANL2DZ	32
TDM Analysis using Functional: wB97XD Basis Set: LANL2DZ.....	35
TDM analysis using the wB97XD functional and the DEF2SVP basis set	38
Visualizations of select IR modes.....	41
Crystallographic Data	45
X-ray Photoelectron Spectroscopy	47
C1m	47
C2m	48
Quantification of Cl and Ir for C1m.....	49
DFT Optimized xyz coordinates (Functional: wB97XD Basis Set: DEF2SVP).....	50
DFT optimized xyz coordinates for C1m Cl down	50
DFT optimized xyz coordinates for C1m Cl up	52
DFT optimized xyz coordinates for C2m Cl down	53
DFT optimized xyz coordinates for C2m Cl up.....	55
Reported densities of Ir piano-stool complexes.....	58
References.....	58

Experimental Methods

Simulated isotropic IRRAS spectra. The method for the simulation of isotropic IRRA spectra from transmission spectra of C1 and C2 followed previous literature precedent.¹⁻⁸ Briefly, the simulation of isotropic IRRA spectra requires the known experimentally determined molar absorptivity, refractive index, and estimated molecular density, surface coverage, and monolayer thickness of the analyte and the refractive index and molar absorptivity of the Au surface. The molar absorptivity is determined from a transmission FTIR spectra of C1 and C2 were obtained on KBr pellets of known concentrations and thickness (Figure SX). The refractive index is determined via the Kramers-Kronig transformation following molar absorptivity determination (Figure SX). The molecular density of C1 and C2 is estimated from the C3 crystal structure. While this is a starting point for the estimation of the density of C1 and C2, calculated spectra were also made using a high (2.0 g/cm³) and low (1.2 g/cm³) estimation of the density to bracket the determined angle of the transition dipole moments. The high and low estimates were chosen

as 91% of all of Ir piano-stool complexes that contained both a halide and either a 2,2-bipyridine or phenylpyridine moiety in the Cambridge Structural Database had a density between these two values (Figure S45, 78 structures). The surface coverage determined via ICP-MS of the monolayers. The monolayer thickness of C1 and C2 was determined as the average of the distance from the surface and the atom farthest from the surface to the S atom attached to the surface of C1m and C2m monolayers in the Cl up and Cl down orientations in DFT. Spectra was then simulated used methods published elsewhere, using an angle of incidence of the IRRAS as 88° to match the experimental PM-IRRAS.^{1, 7, 8} Overall, due to the estimation of the density, the method has an average tolerance of ±6° (average difference between initial estimation and bracketed high and low values) for the determined angle of the transition dipole moment (TDM).

Comparison of the PM-IRRAS and the Simulated IRRAS via Spectral Fitting. The comparison of the PM-IRRAS and simulated isotropic spectra follows previously reported methods.^{1, 5, 7, 8} Briefly, spectral fits were performed in OriginPro. Following previous lab precedent, all spectra were smoothed with at 9 cm⁻¹ resolution and fit.^{9, 10} Second derivative analysis provided by the OMNIC Series software allowed for the resolution of bands. The PM-IRRAS spectra were fit with Gaussian line shapes and simulated IRRAS spectra where fit with a mixture of Lorentzian and Gaussian line shapes to obtain the most accurate peak areas.^{5, 8, 11, 12}

Determination of Surface Coverage by ICP-MS. Inductively coupled plasma mass spectrometry (ICP-MS) was conducted on a Thermo iCAP RQ ICP-MS instrument with prepared standards and samples. The standards were prepared from an iridium standard with a concentration of 1 µg/ml in 10-20% HCl solution from Acros Organics. Trace metal concentrated HCl (Fisher Chemical) and trace metal concentrated HNO₃ (Fisher Chemical) were used and diluted to the appropriate concentrations. The standards were prepared in 1% HCl with concentrations of 1000 ppb Ir, 100 ppb Ir, 10 ppb Ir, 1 ppb Ir, and 0 ppb. The samples were digested in a 17% HCl solution overnight then diluted with 18.2 MΩ·cm water to a 1% HCl solution for analysis. The digestion Teflon tube was cleaned prior with a 1% HNO₃ solution and left to air dry.

Characterization of SAMs by X-ray photoelectron spectroscopy (XPS).

XPS was done on gold slides prepared identically to the PM-IRRAS and ICP-MS experiments. XPS survey spectra were recorded with a pass energy of 160 eV with a 1 eV step. High-resolution spectra of the Au 4f, C 1s, N 1s, S 2p, Cl 2p, and Ir 4f/Au 5p_{3/2} were recorded with a pass energy of 20 eV. Data processing and analysis was done using CasaXPS. The binding energy of all spectra was energy corrected to the Au 4f_{7/2} line at 84.0 eV as reference. Background correction was carried out using a Shirley background for all signals. High-resolution spectra was fit with a mix of Gaussian and Lorentzian line shapes to obtain the most accurate peak areas.

NMR Spectra

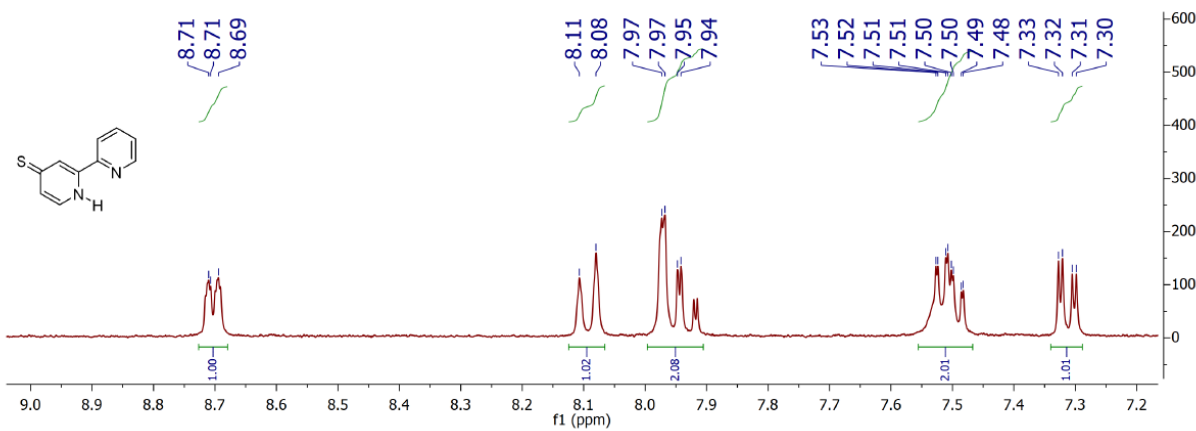


Figure S1. ^1H NMR (300 MHz) spectrum of 4-thione-2,2'-bipyridine in CD_3CN (aromatic region).

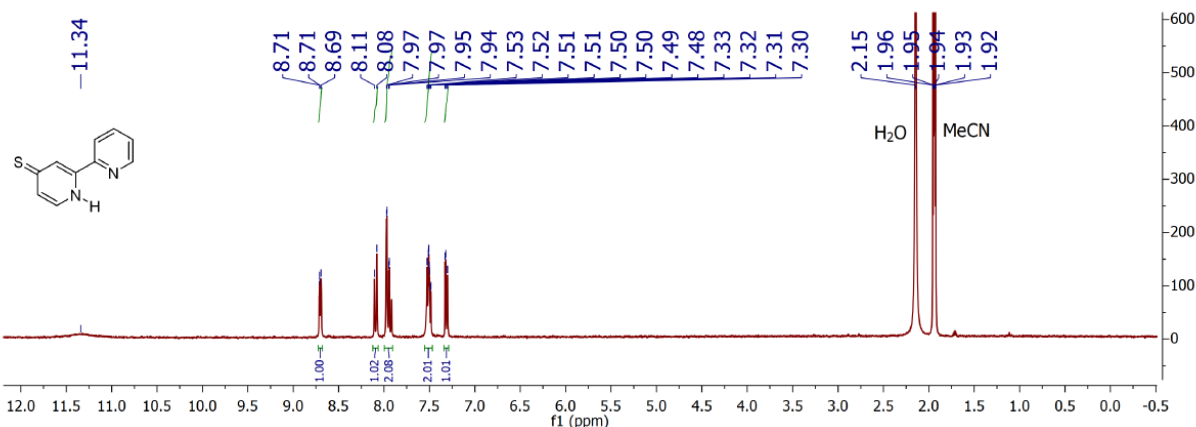


Figure S2. ^1H NMR (300 MHz) spectrum of 4-thione-2,2'-bipyridine in CD₃CN

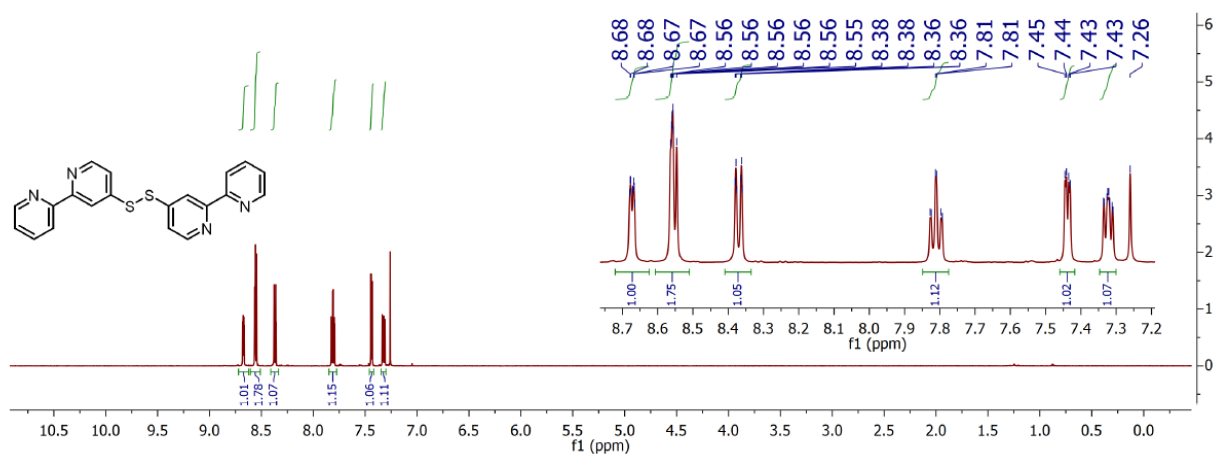


Figure S3. ^1H NMR (500 MHz) spectrum of di(2,2'-bipyridine)-4-disulfide in CDCl_3

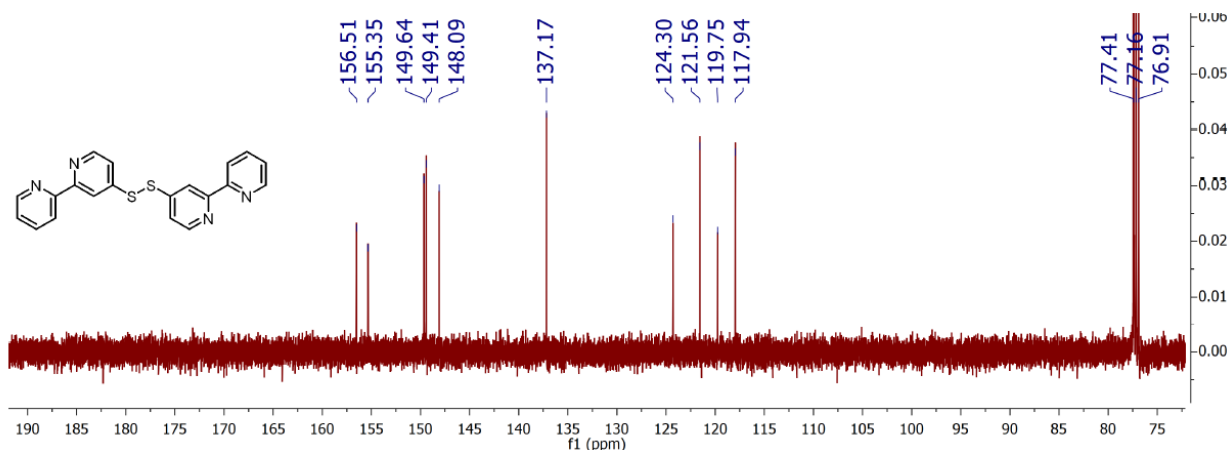


Figure S4. $^{13}\text{C}\{\text{H}\}$ NMR (126 MHz) spectrum of di(2,2'-bipyridine)-4-disulfide in CDCl_3

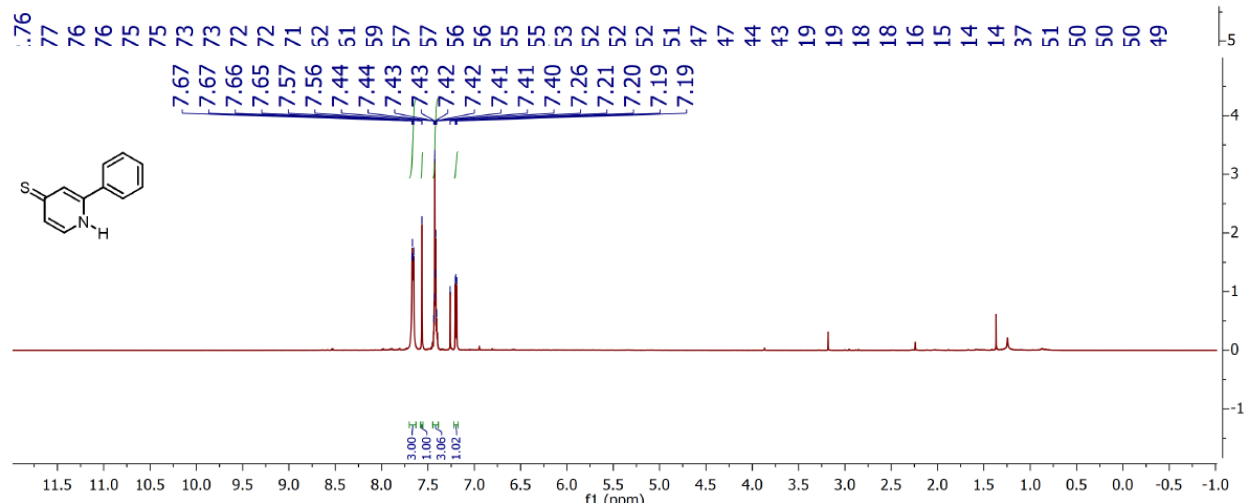


Figure S5. ^1H NMR (500 MHz) spectrum of 4-thione-2-phenylpyridine in CDCl_3

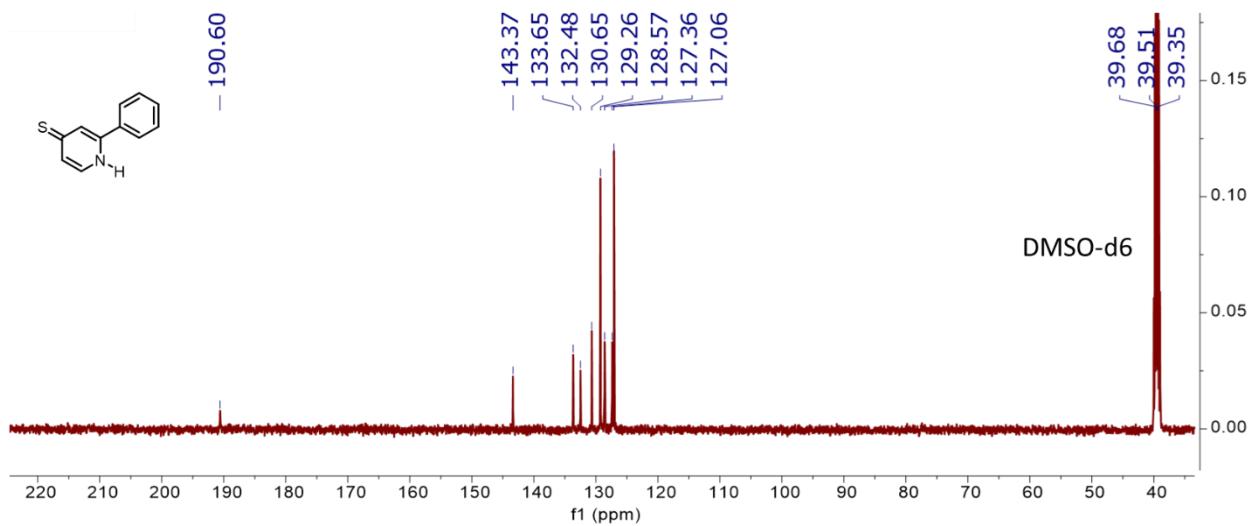


Figure S6. $^{13}\text{C}\{\text{H}\}$ NMR (126 MHz) spectrum of 4-thione-2-phenylpyridine in $(\text{CD}_3)_2\text{SO}$

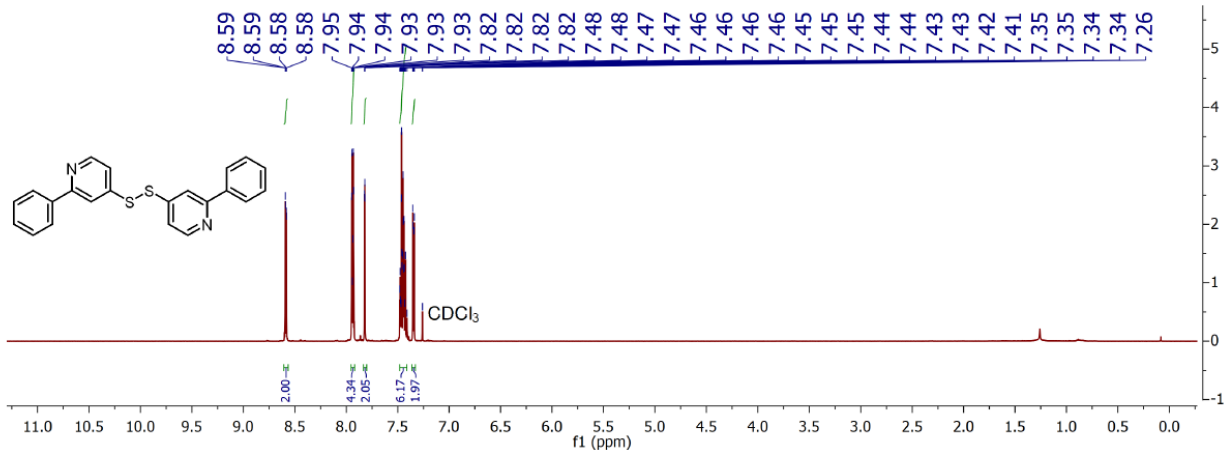


Figure S7. ^1H NMR (500 MHz) spectrum of di(2-phenylpyridine)-4-disulfide in CDCl_3

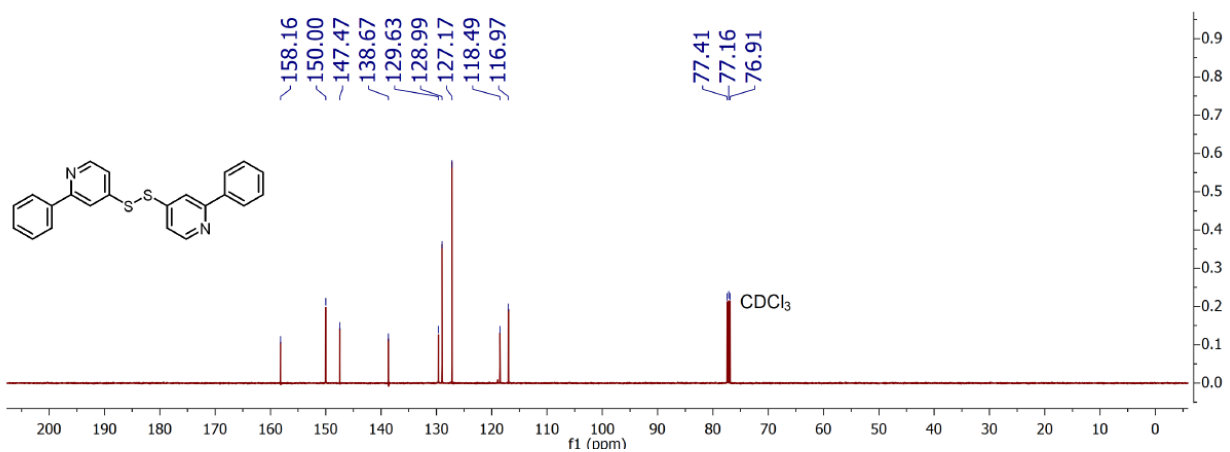


Figure S8. $^{13}\text{C}\{^1\text{H}\}$ NMR (126 MHz) spectrum of di(2-phenylpyridine)-4-disulfide in CDCl_3

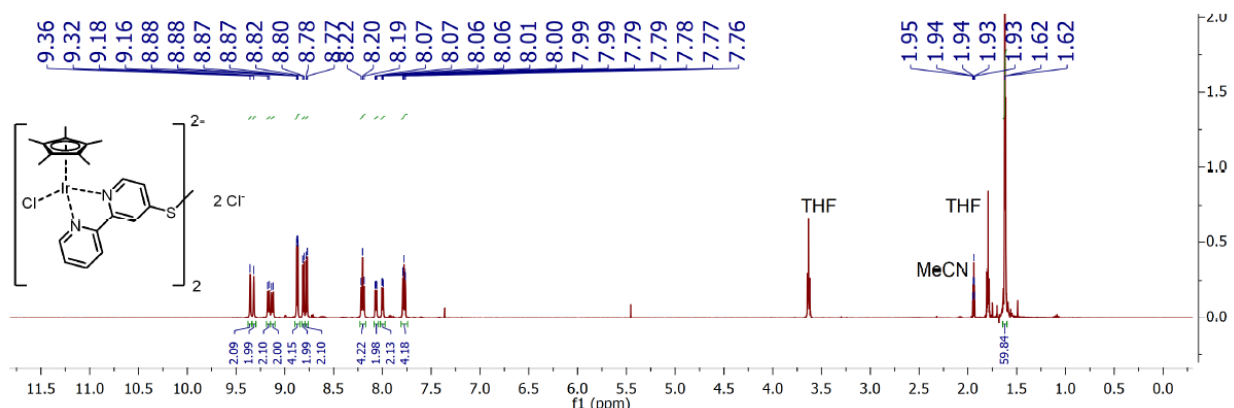


Figure S9. ^1H NMR (500 MHz) spectrum of $\text{C1} [\text{Cp}^*\text{Ir}((2,2'\text{-bipyridine-4-sulfide})\text{Cl}]_2 [\text{Cl}]_2$ (statistical mixture of diastereomers) in CH_3CN

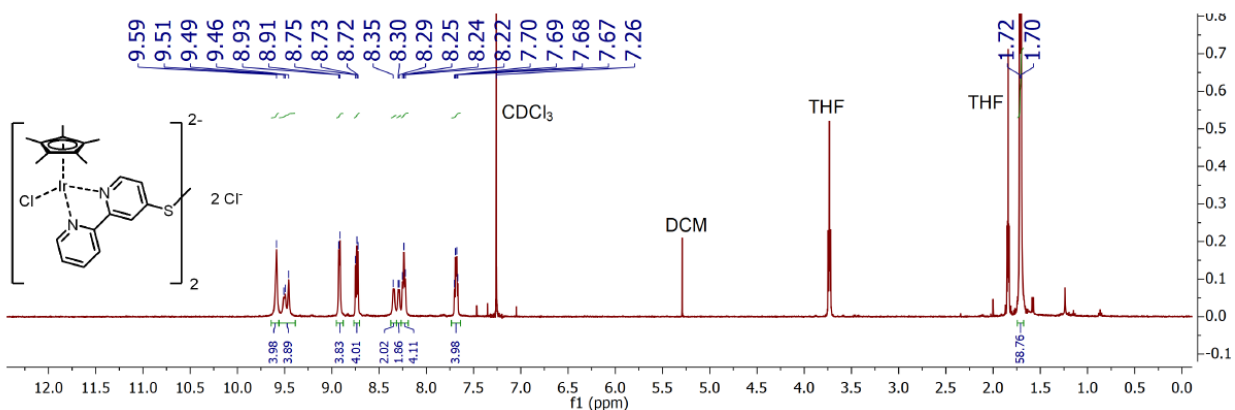


Figure S10. ^1H NMR (500 MHz) spectrum of $\text{C1} [\text{Cp}^*\text{Ir}((2,2'\text{-bipyridine-4-sulfide})\text{Cl}]_2 [\text{Cl}]_2$ (statistical mixture of diastereomers) in CDCl_3

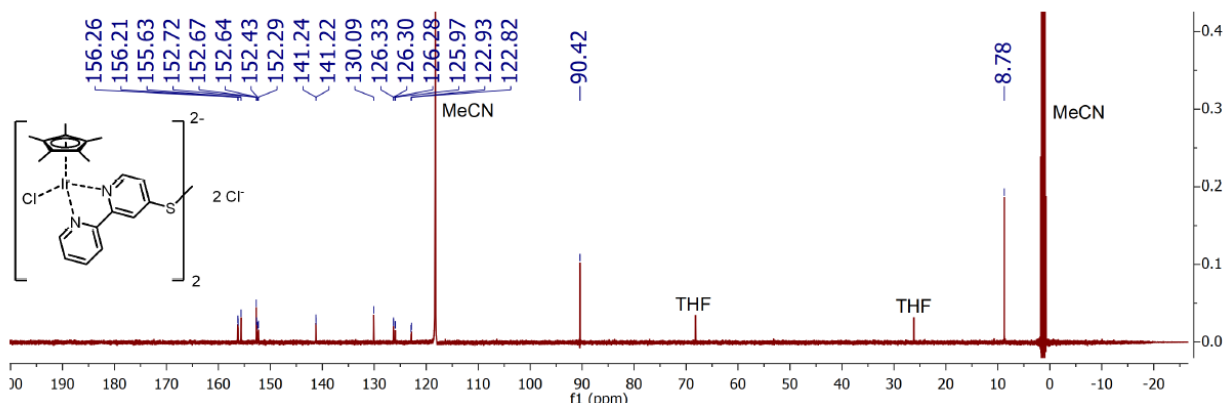


Figure S11. $^{13}\text{C}\{^1\text{H}\}$ NMR (126 MHz) spectrum of $\text{C1} [\text{Cp}^*\text{Ir}((2,2'\text{-bipyridine-4-sulfide})\text{Cl}]_2 [\text{Cl}]_2$ (statistical mixture of diastereomers) in CD_3CN

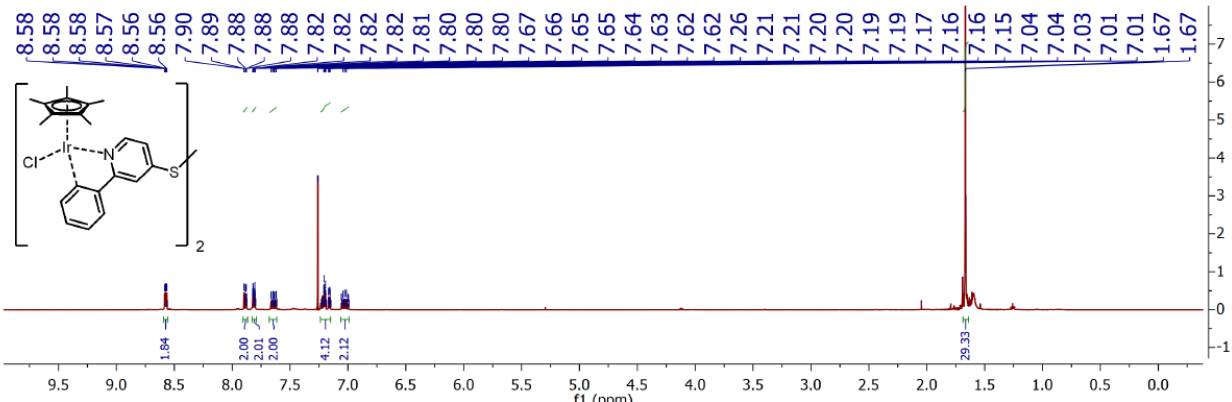


Figure S12. ^1H NMR (500 MHz) spectrum of **C2** [$\text{Cp}^*\text{Ir}(2\text{-phenylpyridine-4-sulfide})\text{Cl}]_2$ (statistical mixture of diastereomers) in CDCl_3

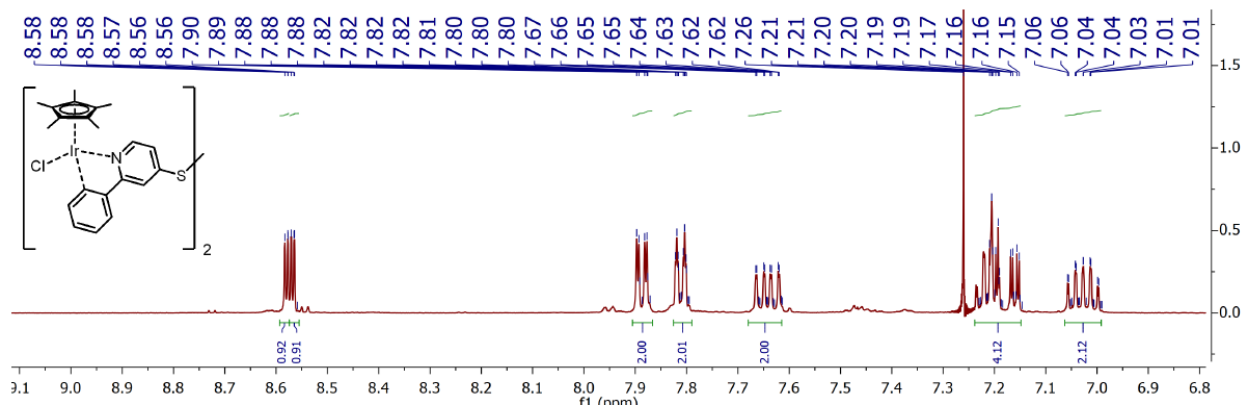


Figure S13. ^1H NMR (500 MHz) spectrum of **C2** [$\text{Cp}^*\text{Ir}(2\text{-phenylpyridine-4-sulfide})\text{Cl}]_2$ (statistical mixture of diastereomers) in CDCl_3 (aromatic region).

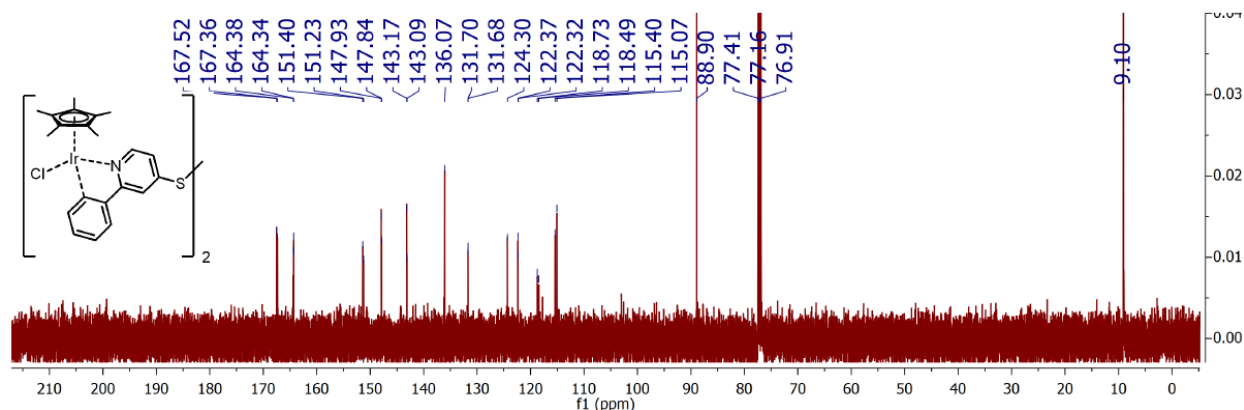


Figure S14. $^{13}\text{C}\{\text{H}\}$ NMR (126 MHz) spectrum of **C2** [$\text{Cp}^*\text{Ir}(2\text{-phenylpyridine-4-sulfide})\text{Cl}]_2$ (statistical mixture of diastereomers) in CDCl_3

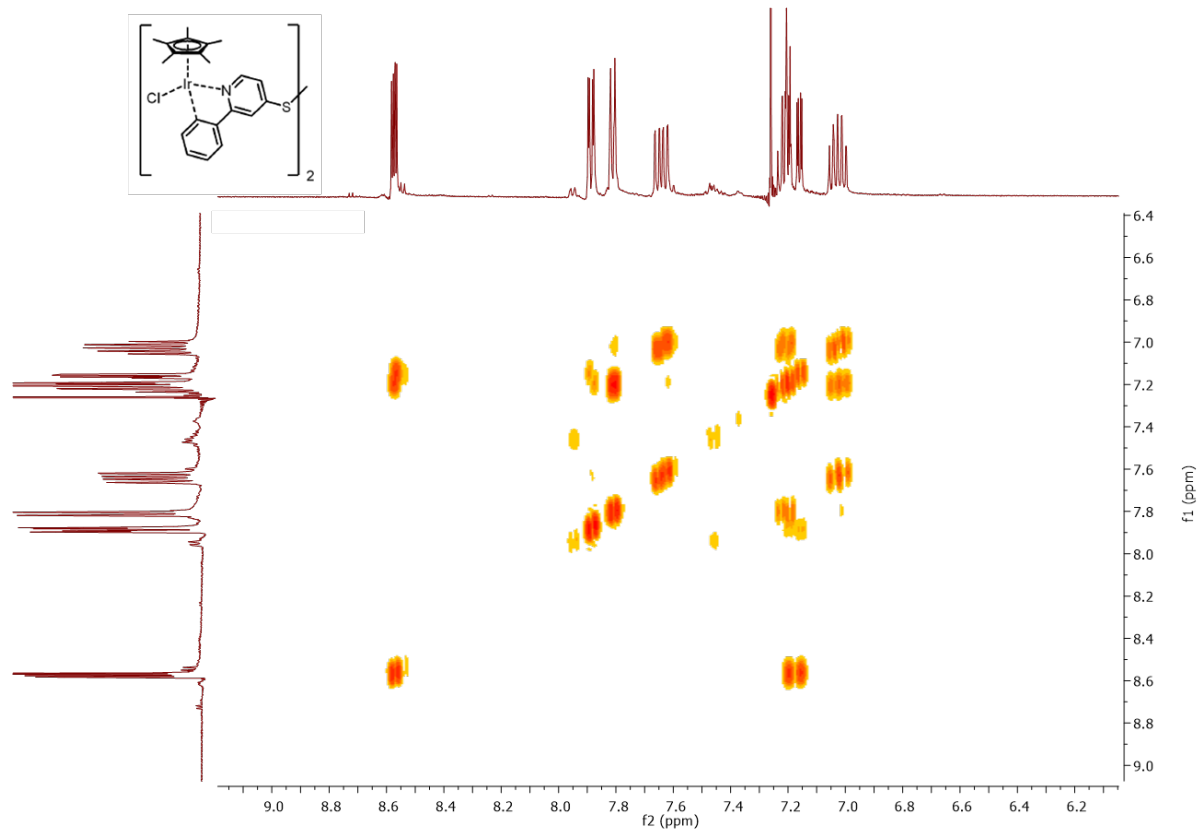


Figure S15. COSY NMR (500 MHz) spectrum of **C2** [$\text{Cp}^*\text{Ir}(2\text{-phenylpyridine-4-sulfide})\text{Cl}]_2$ (statistical mixture of diastereomers) in CDCl_3

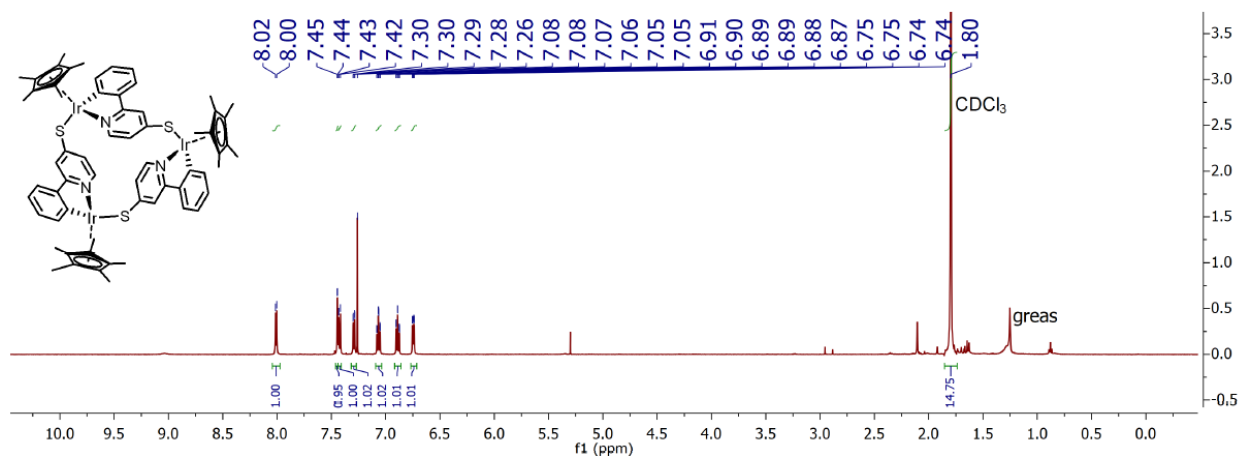


Figure S16. ${}^1\text{H}$ NMR (500 MHz) spectrum of **C3** [$\text{Cp}^*\text{Ir}(2\text{-phenylpyridine-4-thiol})]_3$ in CDCl_3

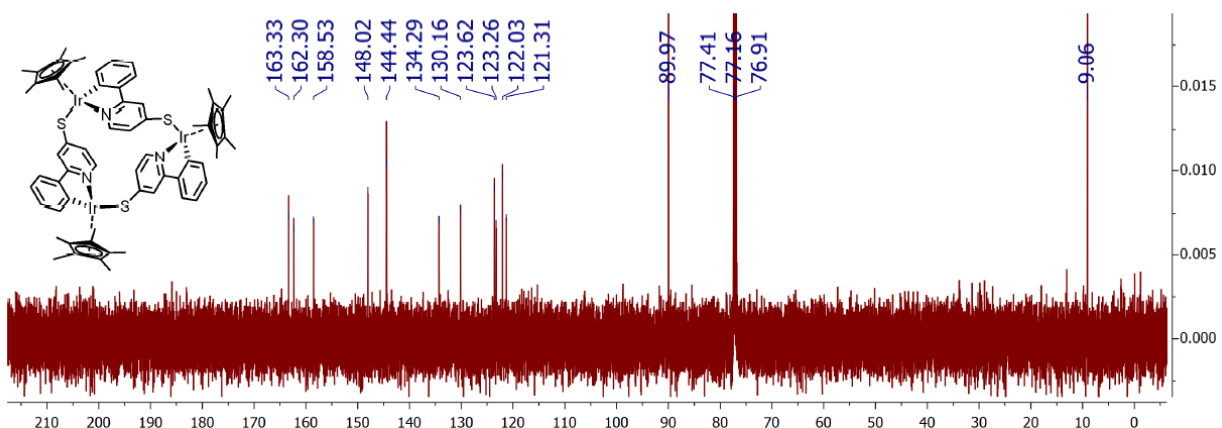


Figure S17. $^{13}\text{C}\{^1\text{H}\}$ NMR (126 MHz) spectrum of **C3** [$\text{Cp}^*\text{Ir}(2\text{-phenylpyridine-4-thiol})_3$] in CDCl_3

IR-Spectra

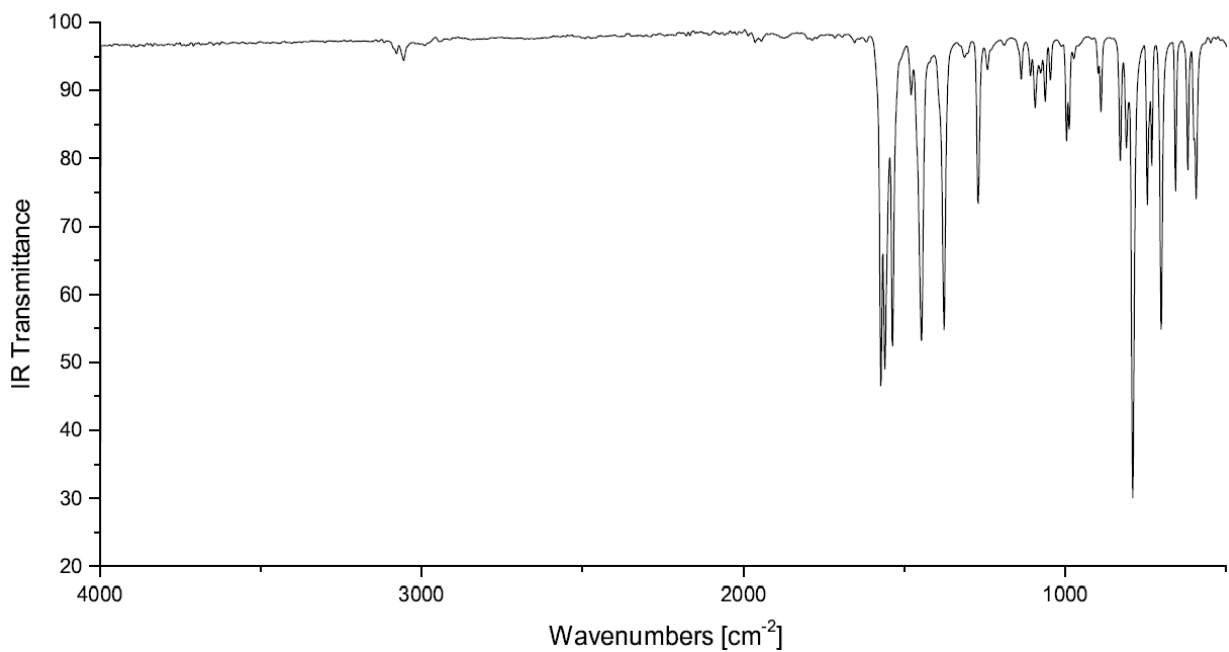


Figure S18. FT-IR (ATR) spectrum of di(2,2'-bipyridine)-4-disulfide

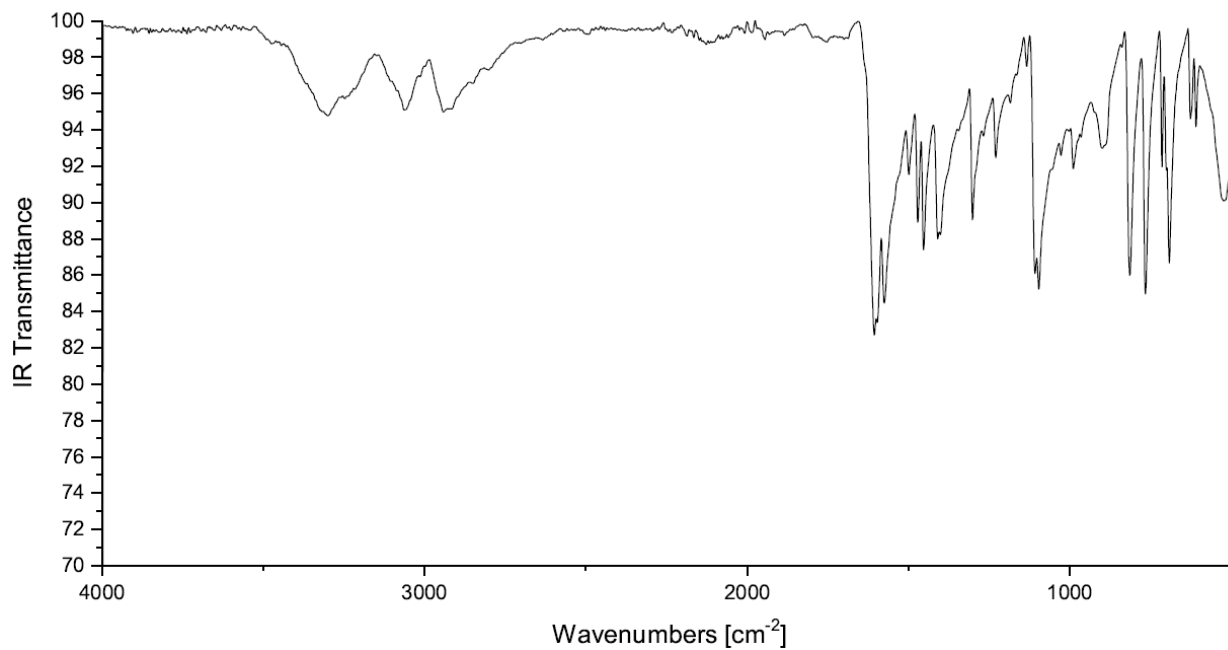


Figure S19. FT-IR (ATR) spectrum of 4-thione-2-phenylpyridine

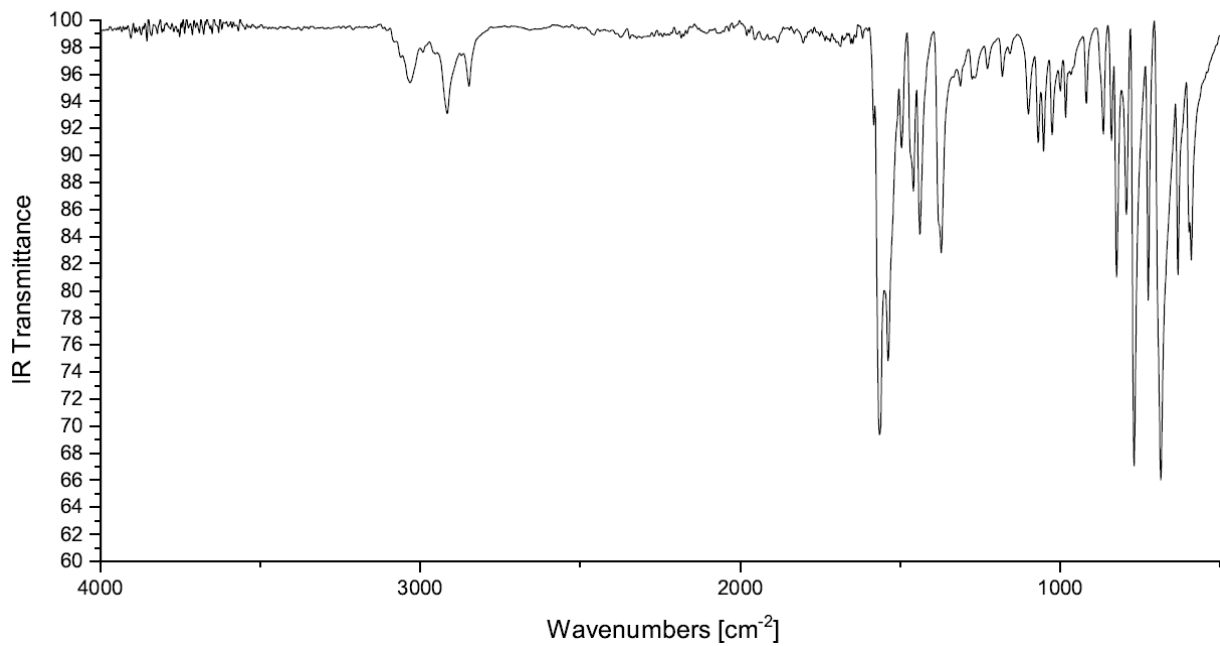


Figure S20. FT-IR (ATR) spectrum of di(2-phenylpyridine)-4-disulfide

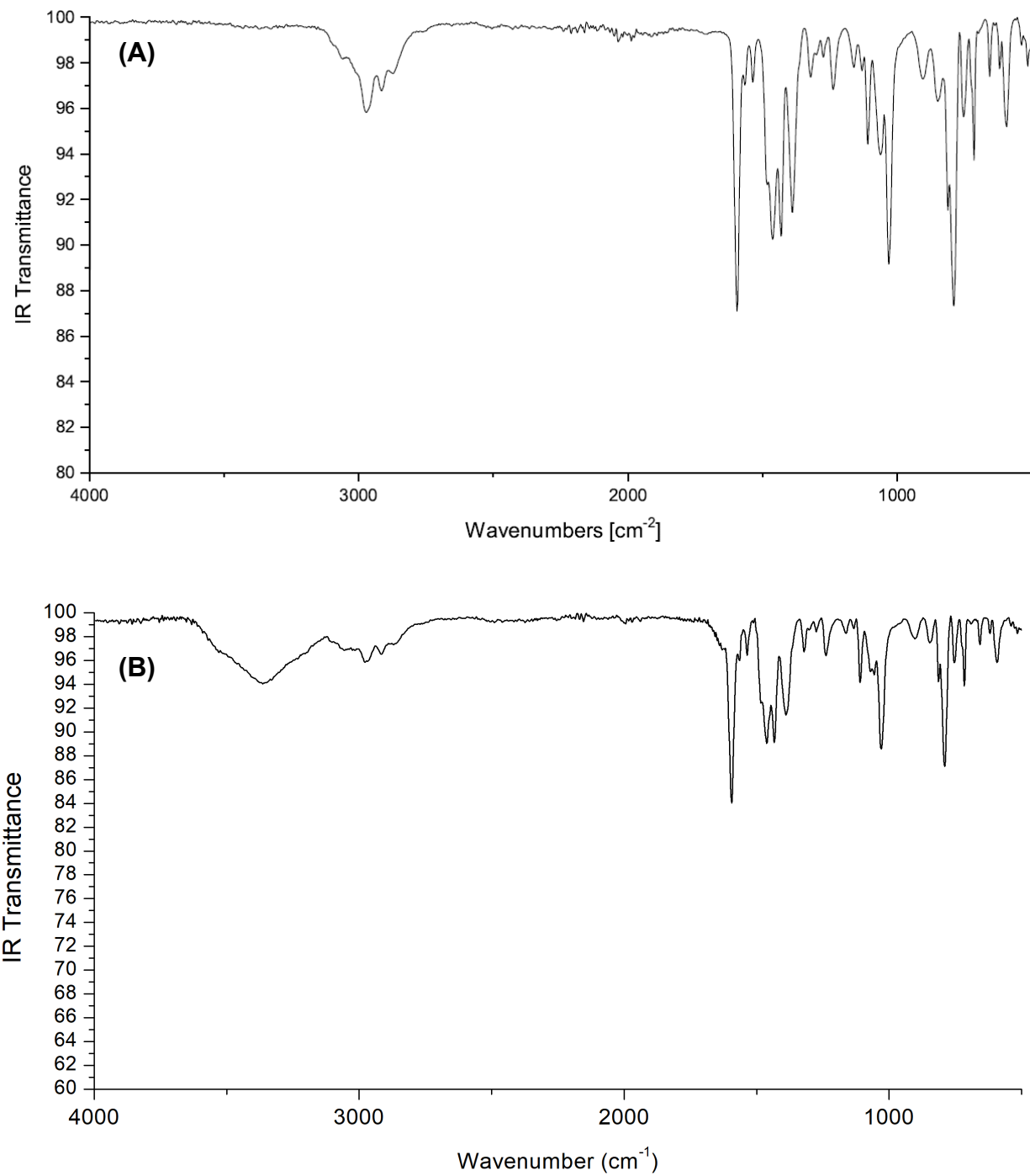


Figure S21. FT-IR (ATR) spectrum of **C1** [$\text{Cp}^*\text{Ir}((2,2'\text{-bipyridine-4-sulfide})\text{Cl}]_2\text{Cl}_2$ in (A) in inert atmosphere and (B) in air following removal from the glovebox. (B) shows a broad water peak as a result of the hydroscopic nature of **C1**.

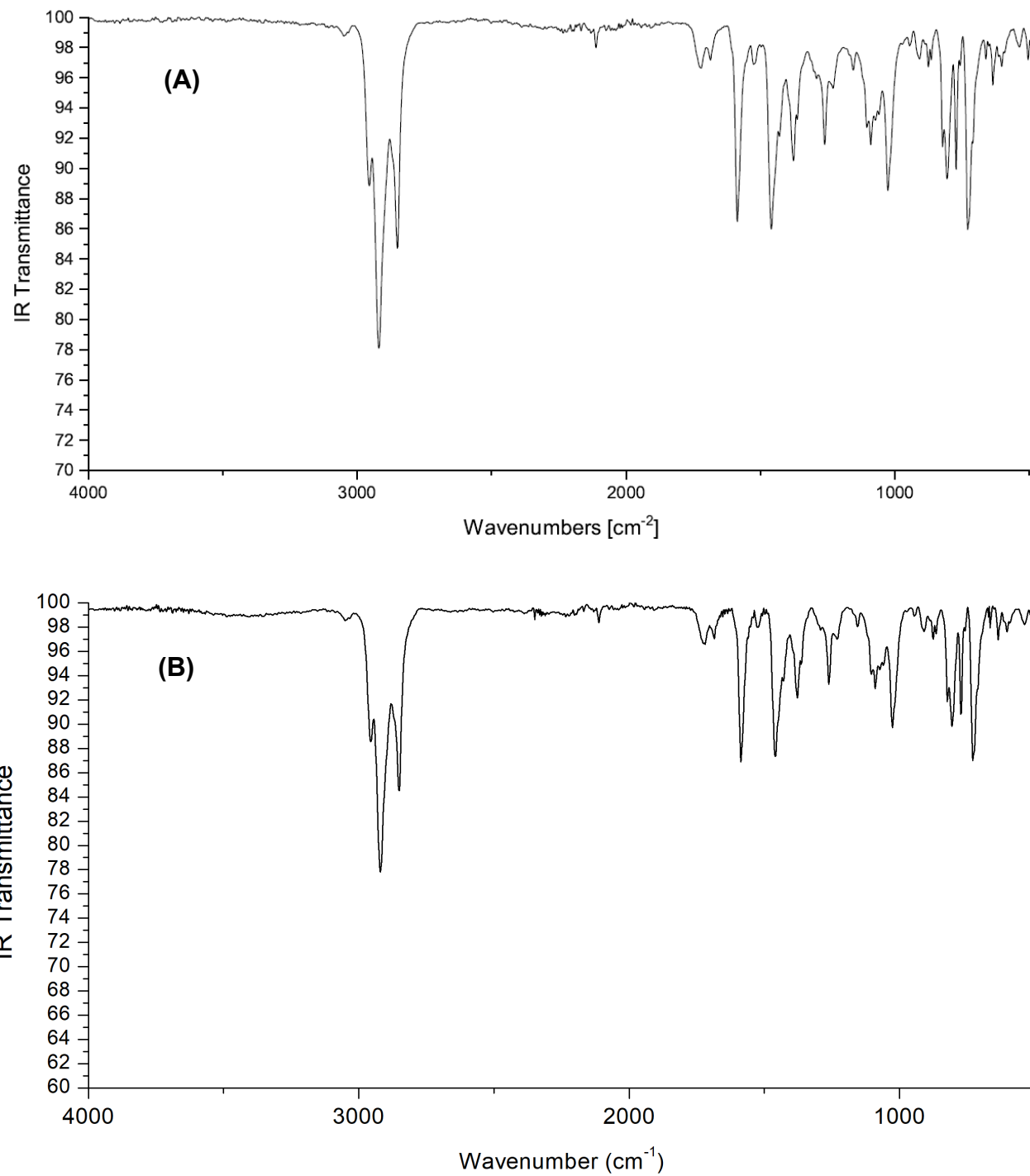


Figure S22. FT-IR (ATR) spectrum of C2 [$\text{Cp}^*\text{Ir}(2\text{-phenylpyridine-4-sulfide})\text{Cl}_2$] (A) in the glovebox and the same sample (B) shows small, broad water peak showing that C2 is a little hygroscopic.

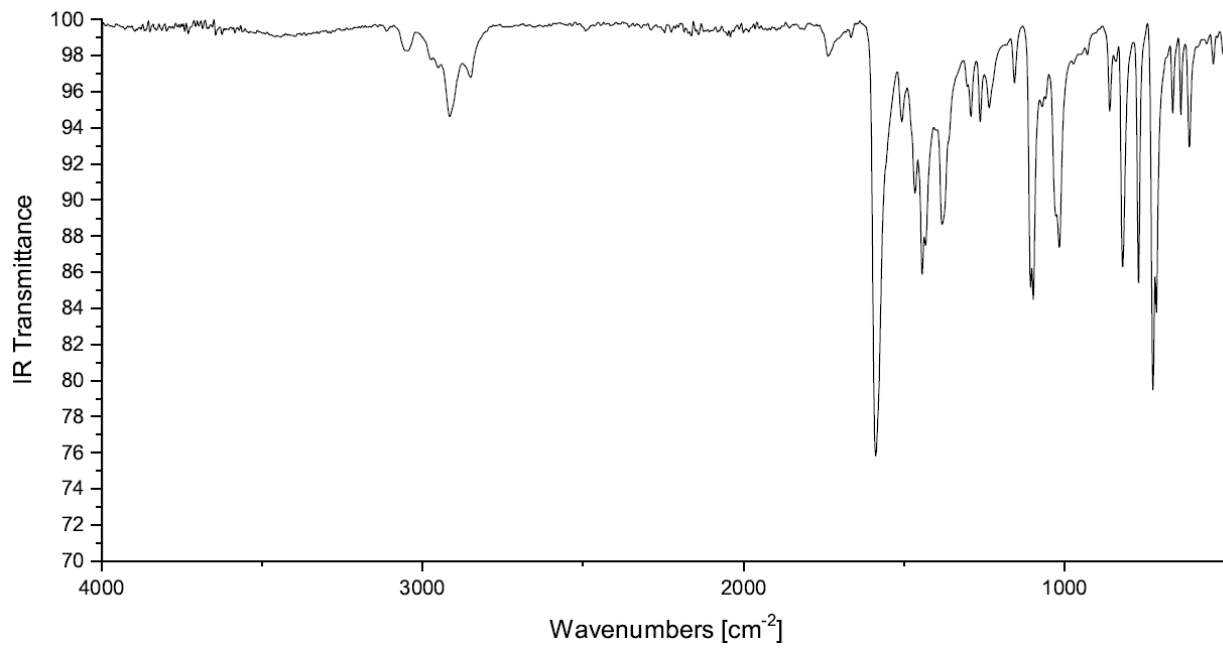


Figure S23. FT-IR (ATR) spectrum of **C3** [$\text{Cp}^*\text{Ir}(2\text{-phenylpyridine-4-thiol})_3$]

FTIR Spectra of KBr Pellets

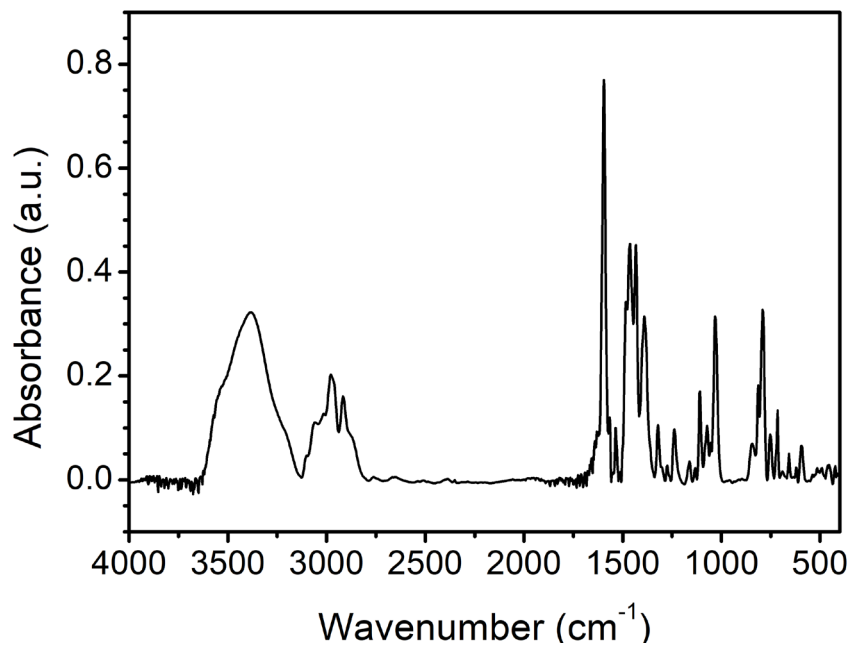


Figure S24. FTIR of **C1** in a KBr pellet in air.

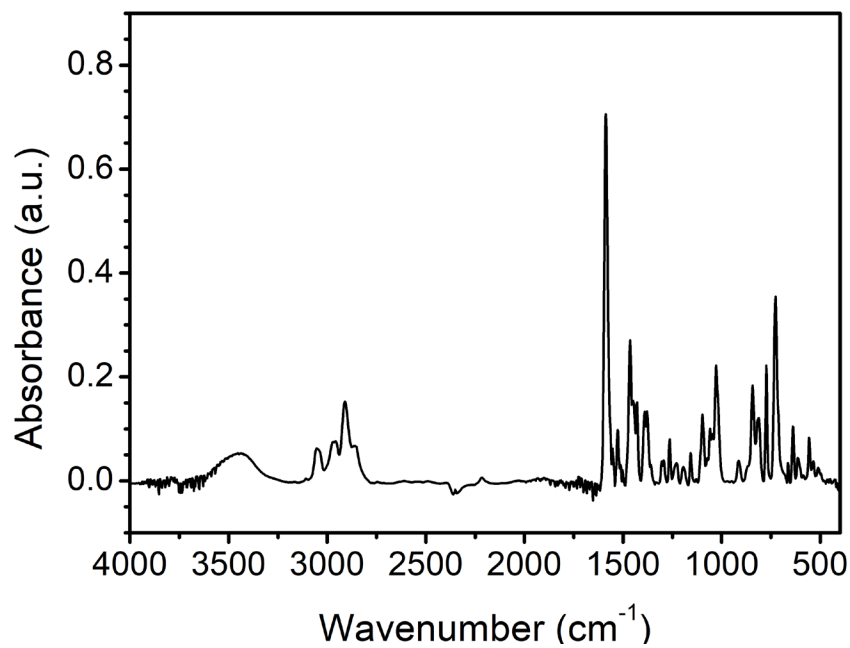


Figure S25. FTIR of **C2** in a KBr pellet in air.

Molar Absorptivity and Refractive Index

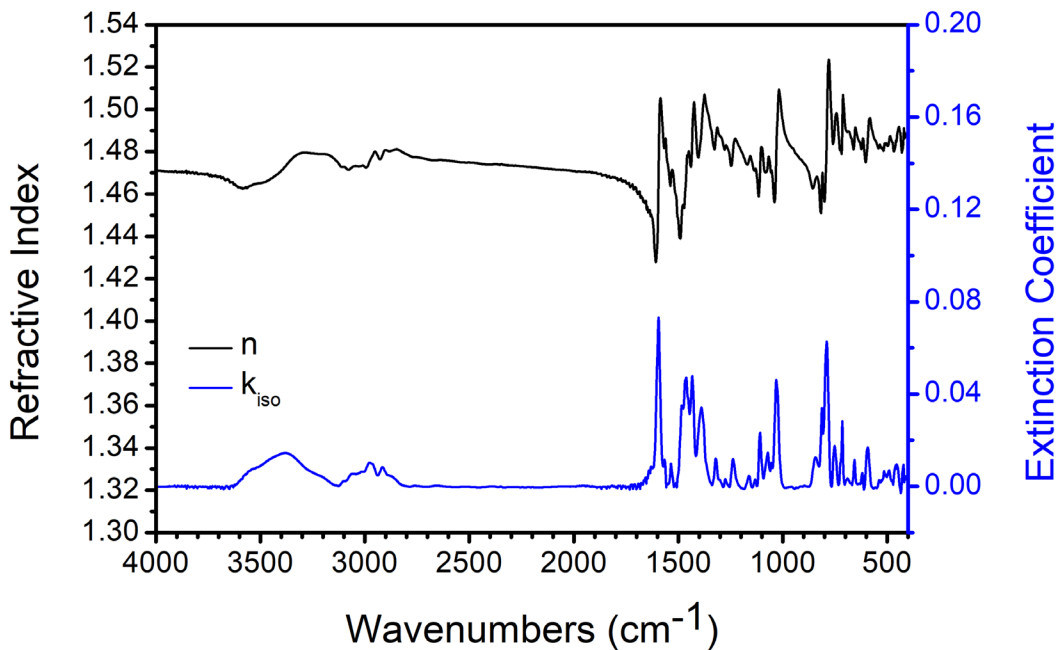


Figure26. Extinction coefficient, k_{iso} , of **C1** obtained from IR-transmission spectroscopy. Refractive index, n , of **C1** obtained from the Kramers-Krnoig transformation of k .

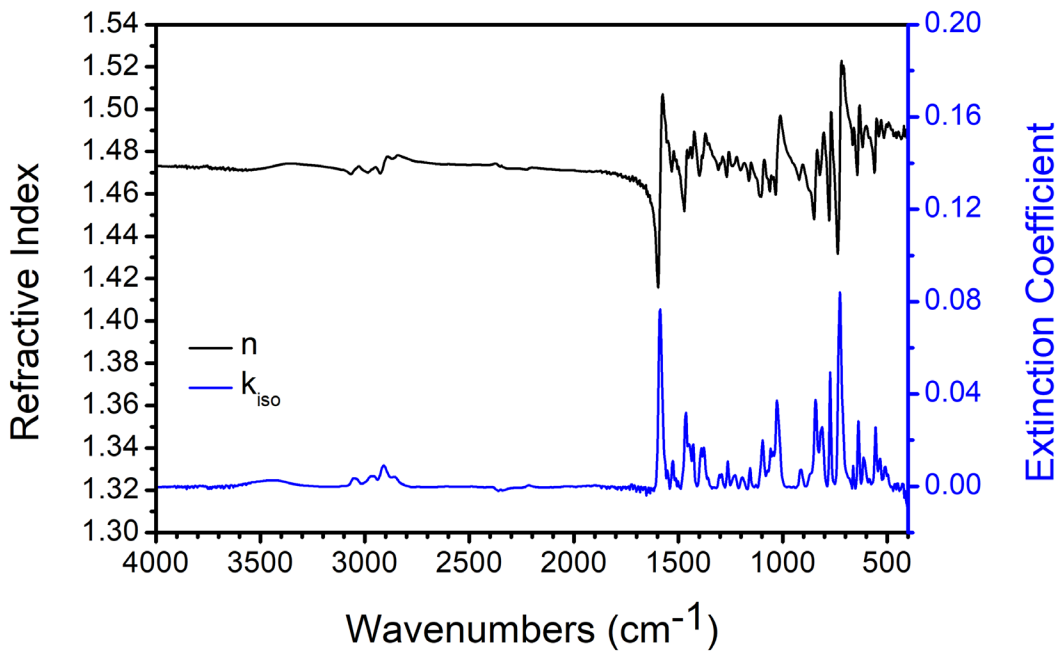


Figure S27. Extinction coefficient, k_{iso} , of **C2** obtained from IR-transmission spectroscopy. Refractive index, n , of **C2** obtained from the Kramers-Krnoig transformation of k .

Mass Spectra

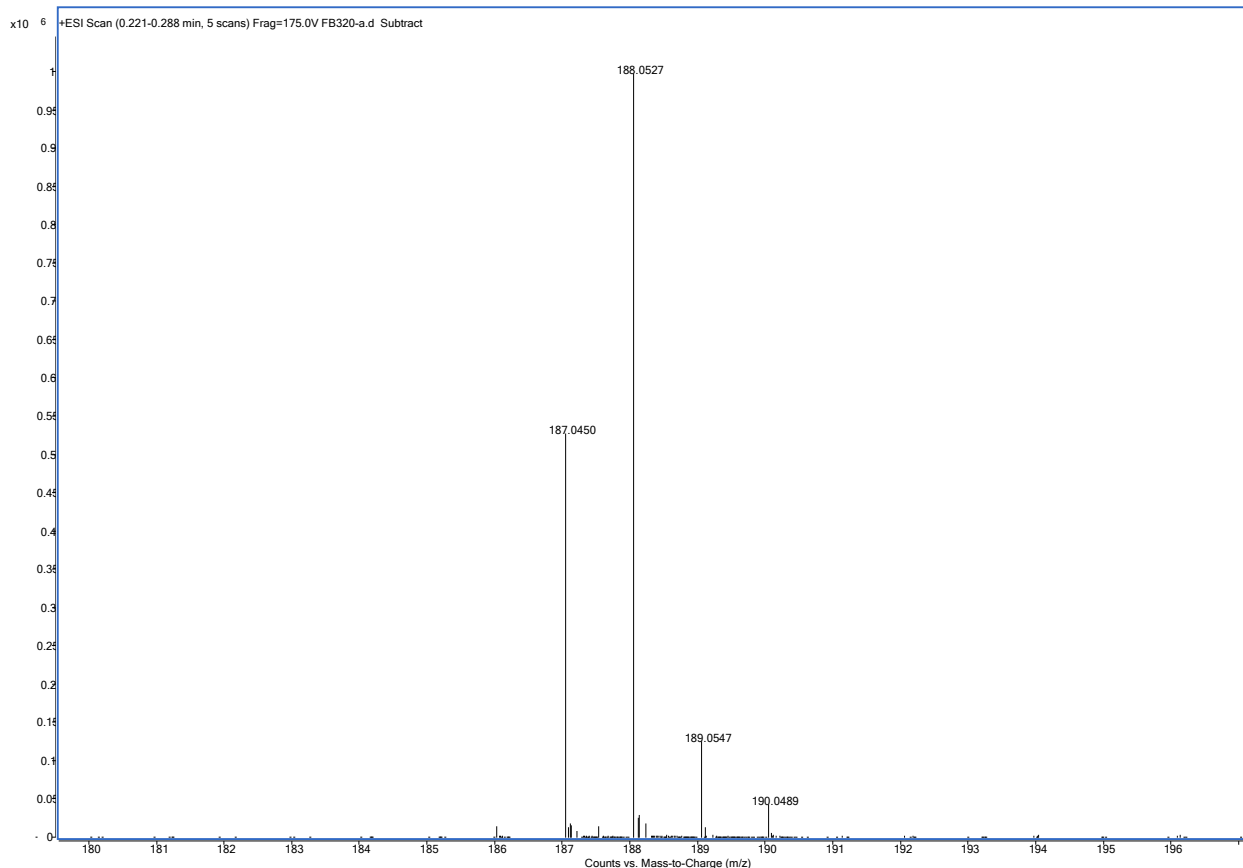


Figure S28. Measured HR-ESI-MS for 4-thione-2-phenylpyridine (**ppy=S**). m/z calcd for $[M]^+$ 188.0527 (found) 188.052; calcd for $[M + H]^+$ 187.0450 (found) 187.0450.

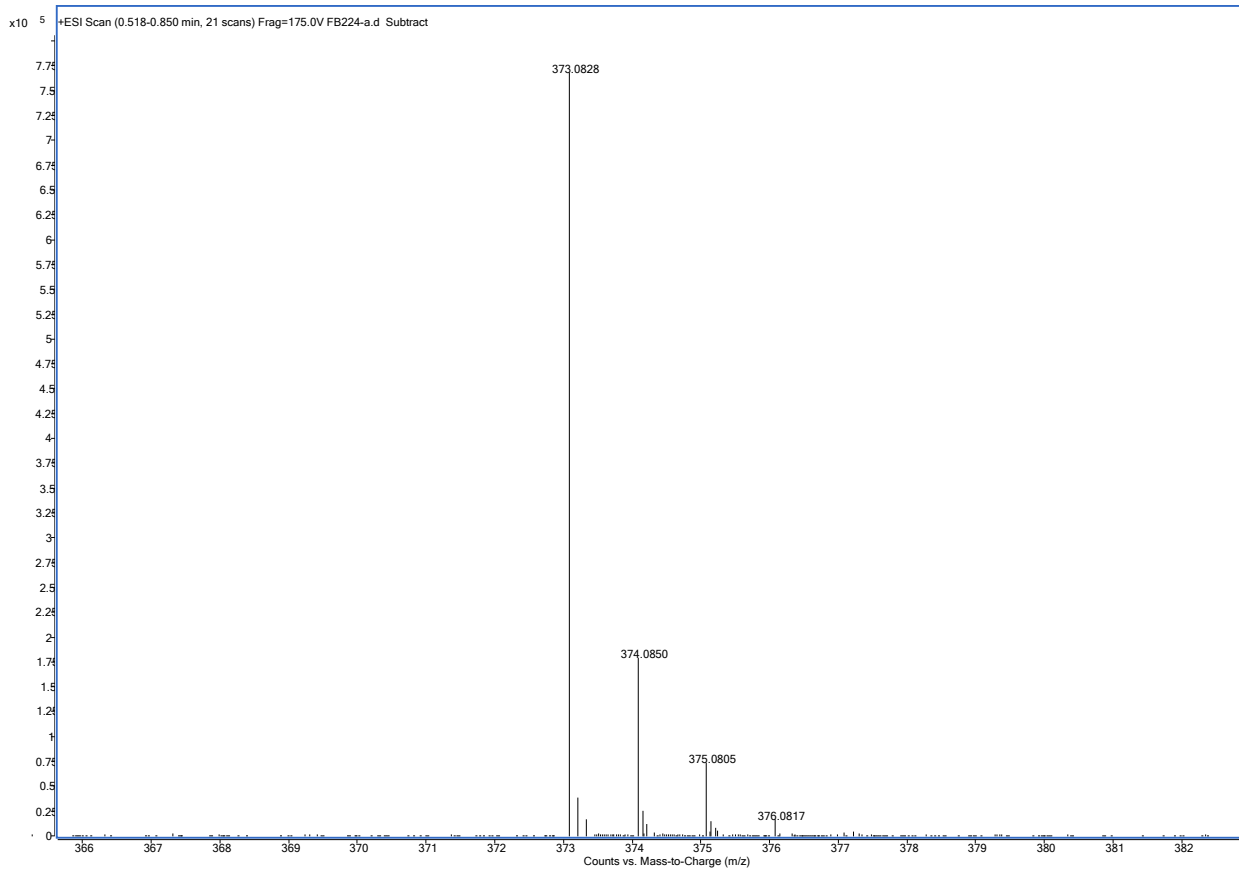


Figure S29. Measured HR-ESI-MS for di(2-phenylpyridine)-4-disulfide (**ppySSppy**). m/z calcd for $[M + H]^+$ 373.0828 (found) 373.0828.

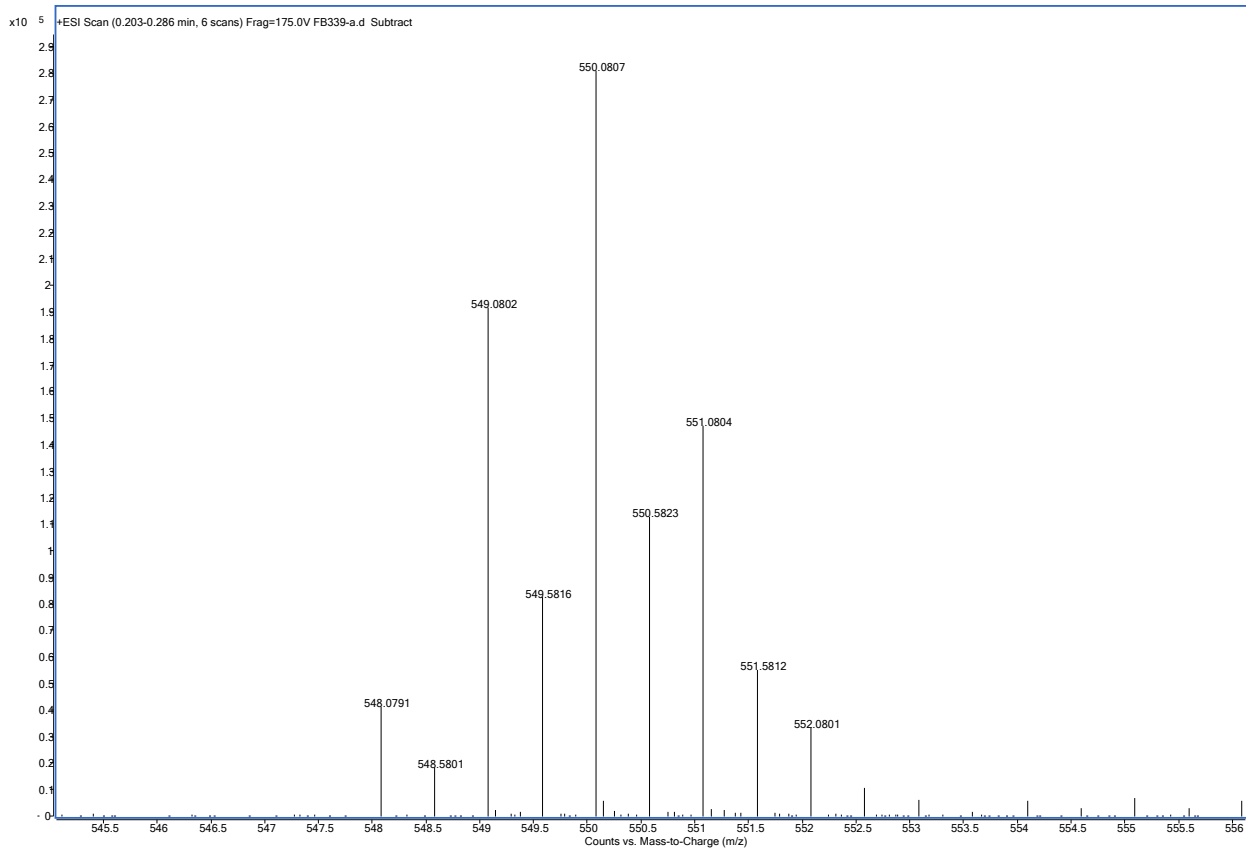


Figure S30. Measured HR-ESI-MS of C1 ($[M-2Cl]^{2+}$).

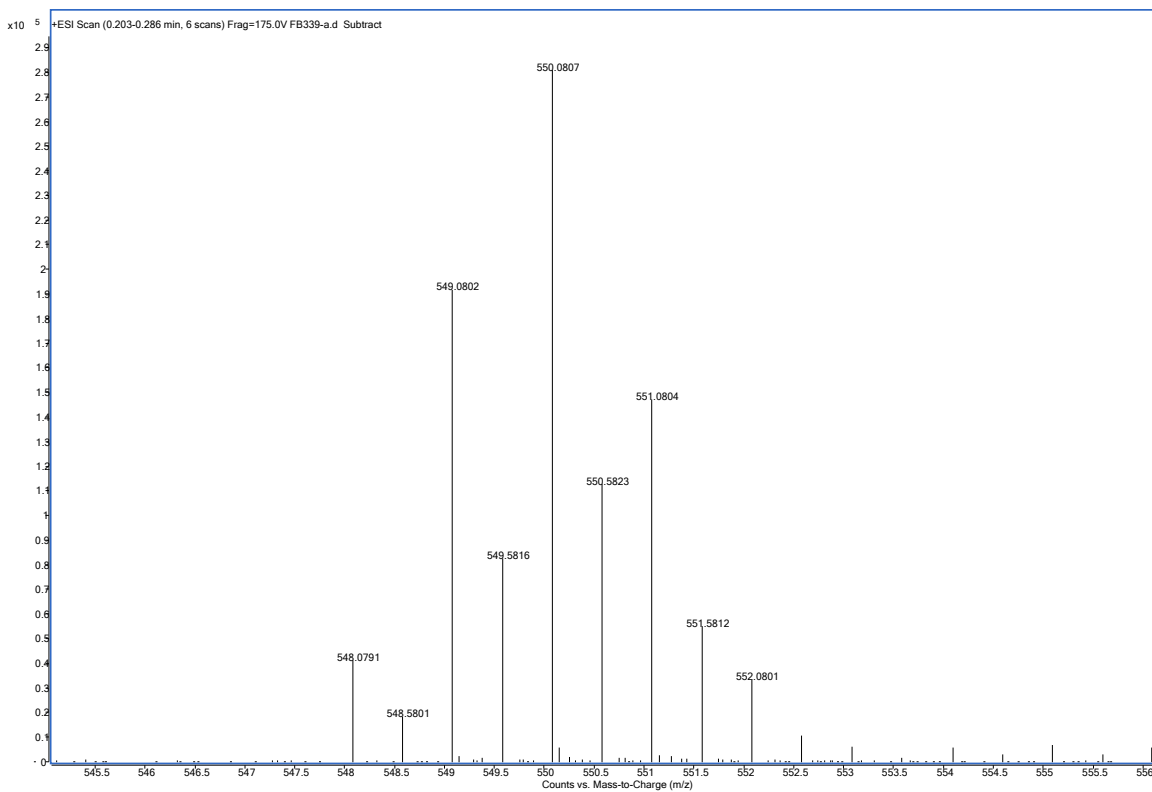


Figure S31. Measured high-resolution mass spectra of **C2** ($[M-2Cl]^{2+}$).

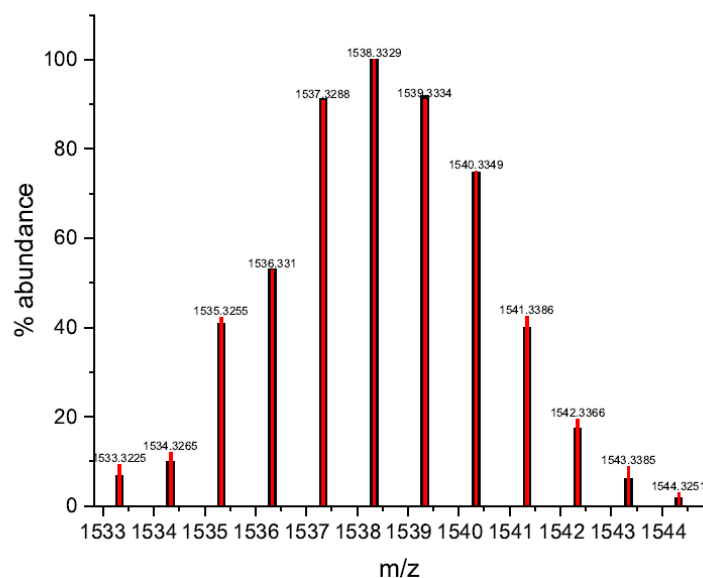


Figure S32. Measured high-resolution mass spec of **C3** (red) and linear combination of calculated mass spec of $[M]^+$ / $[M + H]^+$ at a ratio of 58% / 42% (black).

ICP-MS determination of surface coverage

Table S1. Variables used in the determination of complex surface coverage using inductively-coupled plasma mass spectrometry.

	C1	C2
Au slide dimensions	0.85cmx1cm	2x1.2cm
Digested Solution Mass (kg)	0.0110634	0.01563852
Ir concentration in digestion (ppb)	18.4613	6.4887
Ir determined (mol)	1.06256E-09	5.279E-10
Surface Coverage (mol/cm ²)	1.25007E-09	2.19958E-10

Parameters for IRRAS Simulation

Table S2. Variables used in simulation of the IRRAS spectra from the KBr of the complex using the Kramers-Kronig transformation.

	C1	C2
KBr Mass (g)	0.4106	0.4075
Modifier Mass (g)	0.0014	0.0025
Pellet Mass (g)	0.2208	0.1088
Pellet KBr mass (g)	0.2200	0.1081
Pellet Compound Mass (g)	0.0008	0.0007
KBr Pellet Thickness (cm)	0.228	0.119
Volume KBr Pellet (cm ³)	0.0910	0.0475
Density (g/cm ³)	1.555	1.555
Molar Mass (g/mol)	1171.17	1096.28
Pure Molar Concentration (C ₀) in mol/cm ³	0.001328	0.001418
Molar Concentration in KBr (C) in mol/cm ³	7.0375E-06	1.2737E-05
k' -> k conversion (C ₀ /C)	188.67	111.36
Surface Coverage Γ (molecules/cm ²)	7.528E+14	1.325E+14
Monolayer Thickness (cm)	8.341E-08	8.391E-08

Raw PM-IRRAS

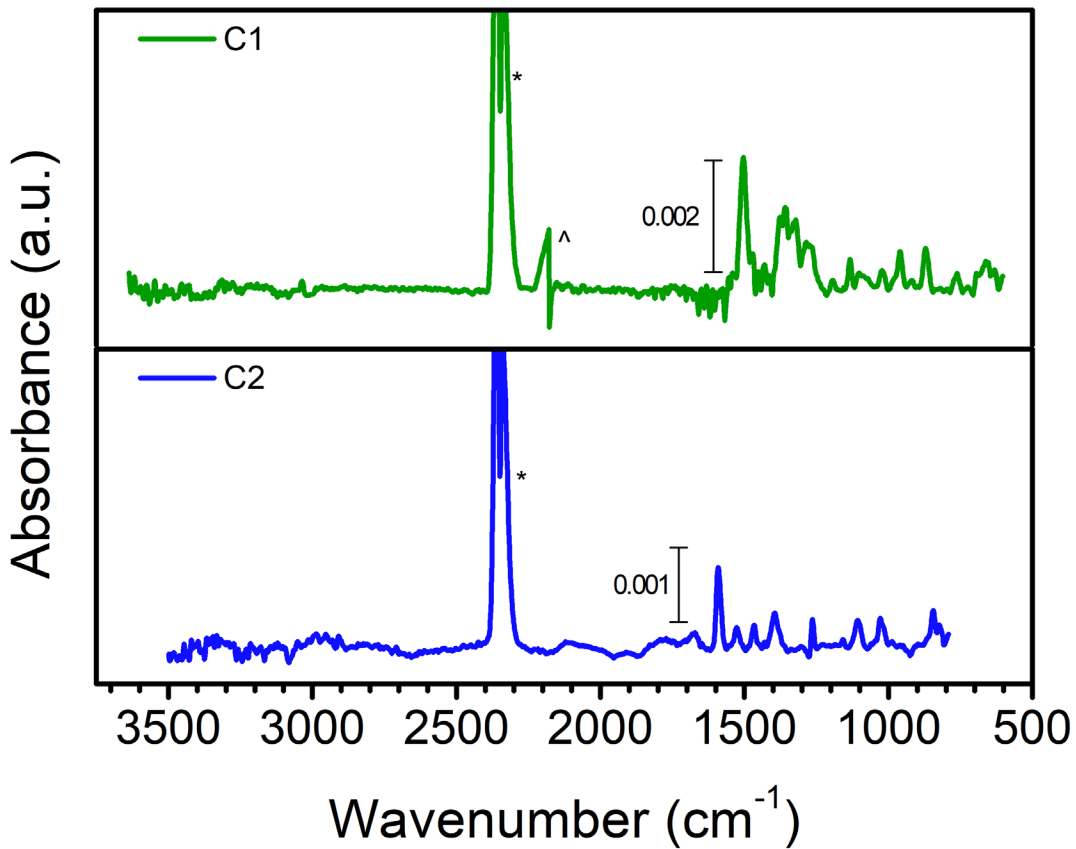


Figure S33. PM-IRRAS of C1 (green) and C2 (blue) on Au. Figure is combined spectra taken with maximum dephasing at 3000 cm^{-1} and 1600 cm^{-1} to minimize PM error across the entire spectra. * indicates atmospheric CO_2 and ^ is where the two spectra are combined.

PM-IRRAS and Simulated IRRAS with Fits

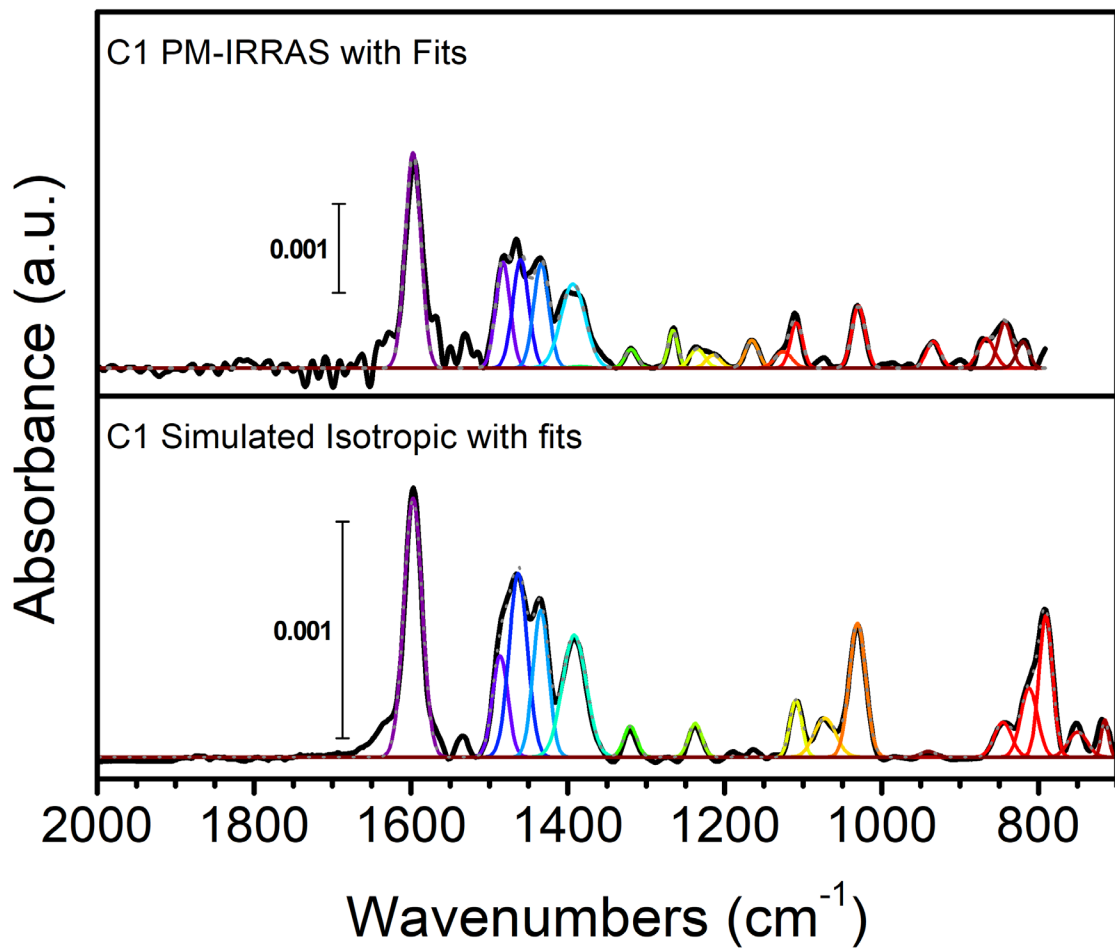


Figure S34. PM-IRRAS (top) and simulated IRRAS (bottom) spectra with fits of a monolayer made from **C1**. The PM-IRRAS spectrum is fit with Gaussian line shapes and the simulated IRRAS spectrum is fit with a combination of Lorentzian and Gaussian line shapes.

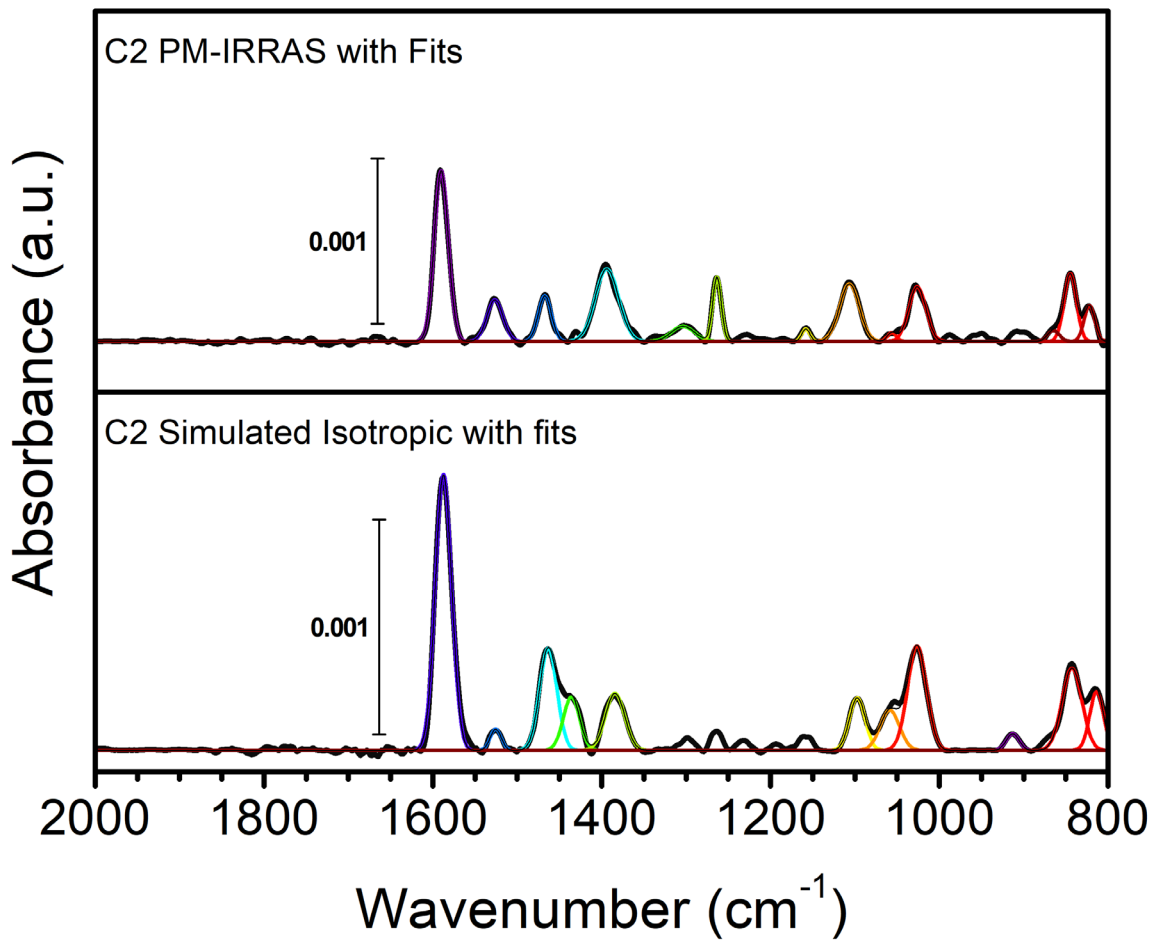


Figure S35. PM-IRRAS (top) and simulated IRRA (bottom) spectra with fits of a monolayer made from **C2** on Au. The PM-IRRAS spectrum is fit with Gaussian line shapes and the simulated IRRA spectrum is fit with a combination of Lorentzian and Gaussian line shapes.

PM-IRRAS Peak Fitting Analysis

Table S3. Vibrational modes and their determined transition dipole moments dependent on the density of the complex used in the simulated IRRA spectra with respect to normal (θ) used for orientation determination of the C1 monolayer on Au.

Peak PM	PM-IRRAS Area	Peak Sim	Sim Area (1.55 g/cm ³)	θ (°)	Sim Area (1.2 g/cm ³)	θ (°) (1.2 g/cm ³)	Sim Area (2.0 g/cm ³)	θ (°) (2.0 g/cm ³)	Transition	Reference
1596	0.0745	1597	0.04283	40	0.03244	29	0.04283	48	bipyridine breathing modes	^{13, 14}
1488	0.02344	1486	0.00919	23	0.00696	0	0.00919	36	C-H bending (bipyridine, Cp*)	¹³
1466	0.02734	1464	0.02861	56	0.02167	50	0.02861	60	C-H bending (Cp*)	¹⁵⁻¹⁸
1441	3.74E-02	1435	0.01922	36	0.01456	22	0.01922	45	C-H bending (Cp*)	¹⁵⁻¹⁸
1390	0.0343	1391	0.01832	38	0.01388	25	0.01832	46	C-H bending (Cp*) Cp* breathing asymmetric	¹⁶⁻¹⁸
1318	0.00252	1320	0.00317	59	0.00241	54	0.00318	63	C-H bending, C-C breathing mix (bipyridine)	¹³
1229	0.00703	1237	0.00359	36	0.00272	22	0.00359	45	C-H bending, C-C breathing mix (bipyridine)	¹³
1110	0.01121	1110	0.00422	20	0.00320	0	0.00422	34	asymmetric C-H bending, C-C breathing mix (bipyridine)	¹³
1075	0.00276	1074	0.00771	70	0.00584	67	0.00771	72	asymmetric C-H bending, C-C breathing mix (bipyridine)	¹³
1027	0.01348	1031	0.01754	60	0.01329	54	0.01754	64	C-H bending (Cp*)	¹⁶⁻¹⁸
944	7.51E-04	940	0.00044	41	0.00033	30	0.00044	49	symmetric C-H bending (Cp*), Cp* vibration mix	¹⁶⁻¹⁸
839	0.00829	845	0.00380	32	0.00288	12	0.00381	42	out of plane C-H bending, bpy	¹³
818	0.00624	813	0.00891	61	0.00675	56	0.00891	65	Bipyridine breathing	¹³

Table S4. Vibrational modes and their determined transition dipole moments dependent on the density of the complex used in the simulated IRRA spectra with respect to normal (θ) used for orientation determination of the C2 monolayer on Au.

Peak PM	PM-IRRAS Area	Peak Sim	Sim Area (1.55 g/cm ³)	θ (°) (1.55 g/cm ³)	Sim Area (1.2 g/cm ³)	θ (°) (1.2 g/cm ³)	Sim Area (2.0 g/cm ³)	θ (°) (2.0 g/cm ³)	Transition	Reference
1589	0.02207	1587	0.03189	61	0.079792	58	0.122355	65	phenylpyridine breathing modes	¹⁹
1526	0.00693	1525	0.00234	7	0.005863	0	0.008991	29	phenylpyridine breathing mode	¹⁹
1476	6.04E-03	1465	0.01190	66	0.029792	63	0.045683	69	C-H bend (Cp*) and Cp* breathing	¹⁵⁻¹⁸
1448	4.84E-04	1451	0.01151	83	0.028816	83	0.044187	84	C-H bend (Cp*)	¹⁶⁻¹⁸
1431	7.95E-04	1428	0.00231	70	0.00578	68	0.008863	73	C-H bend (Cp*, phenylpyridine)	^{16, 17}
1395	0.01445	1390	0.00736	36	0.018424	28	0.028251	44	Cp* breathing, C-H bending (Cp*)	¹⁶⁻¹⁸
1370	1.34E-03	1371	0.00107	50	0.002694	45	0.004131	55	C-H bending symmetric (Cp*)	¹⁶⁻¹⁸
1300	6.12E-04	1299	0.00153	69	0.003837	66	0.005883	71	C-H bending asymmetric (ppy), phenylpyridine breathing mix	This work (DFT)
1227	0.00115	1232	0.00094	50	0.002369	46	0.003632	56	C-H bending asymmetric (ppy)	¹⁹
1186	3.61E-04	1193	0.00062	64	0.00156	61	0.002392	67	C-H bending asymmetric (ppy, Cp*)	This work (DFT)
1158	1.17E-03	1159	0.00178	62	0.004462	59	0.006842	66	C-H bending asymmetric (ppy, Cp*)	This work (DFT)
1104	9.75E-03	1097	0.00565	41	0.014154	34	0.021703	48	C-H bending asymmetric (ppy)	¹⁹
1053	1.23E-03	1060	0.00574	74	0.01437	73	0.022036	76	C-H Methyl wagging (Cp*)	¹⁶⁻¹⁸

1028	7.03E-03	1031	0.01375	66	0.034404	63	0.052756	69	phenylpyridine breathing	^{13, 19}
912	4.41E-04	913	0.00179	73	0.004495	72	0.006893	75	C-H Methyl Wagging asymmetric (Cp*)	^{16, 17}
865	1.29E-03	870	0.00109	51	0.002744	47	0.004208	56	C-H bending ppy out of plane	¹⁹
845	0.00761	845	0.00712	53	0.017815	49	0.027318	58	C-H bending ppy out of plane	^{13, 19}
823	0.00314	838	0.00390	59	0.009775	55	0.014989	63	C-H bending ppy out of plane	^{13, 19}
815	5.20E-04	814	0.00713	81	0.017857	80	0.027382	82	pyridine and phenyl mixed breathing	This work (DFT)

Computational Benchmarking

Benchmarking DFT calculations were performed with the ω B97X-D functional²⁰ as well as the Perdew-Burke-Ernzerhof (PBE) functional²¹ with Grimme's D3 dispersion with Becke-Johnson damping (D3-BJ).²² The inclusion of dispersion was considered to be crucial to correctly describing ligand-Au interactions, and the PBE D3-BJ method had previously been shown to provide accurate and computationally accessible modeling bonds between molecules and Au.²³ Initial calculations were performed with the 6-31G(d,p) basis set²⁴⁻²⁶ on all nonmetal atoms and the LANL2DZ basis set and pseudopotential²⁷ on Ir and Au. Although the minimum energy binding geometries were nearly identical for the two functionals (Table S5, S6 and 1), it was found that the ω B97X-D stretching frequencies and IR intensities (after 0.9485 correction) showed much better agreement with the experiment (Figure S35 and S36). This was particularly evident for the highest intensity mode at \sim 1600 cm⁻¹ corresponding to a bpy breathing mode; this peak showed low intensity using PBE D3-BJ, but was the most intense peak using ω B97X-D. Given the poor agreement of the PBE D3-BJ spectrum, only the ω B97X-D functional was used for further calculations with the larger DEF2SVP basis set and pseudopotential²⁸ on Ir and Au (Tables S11 and S12). These results were relatively similar to the LANL2DZ results but were used for all analysis in the main text since they corresponded to a larger, more polarizable metal basis set.

Comparison of the Experimental and DFT calculated TDMs for orientation determination. To determine the orientation of the monolayers on the Au surface, a comparison between the experimentally determined TDM and DFT (ω B97X-D functional, DEF2SVP basis set) calculated TDM moments. Due to resolution limitations, the peaks determined experimentally correspond to multiple transitions calculated by DFT. Following literature precedent,²⁹ by considering all of the possible TDM calculated for a select mode with the experimentally determined data with similar energy, a comparison can be made. For example, the experimentally determined angle of the transition dipole moment for the bipyridine breath mode was determined to be 40° off normal. DFT calculated 4 bipyridine breathing modes. The average for the 4 transitions is about 26° for the Cl down and 20° for the Cl up orientation.

DFT Computed FTIR

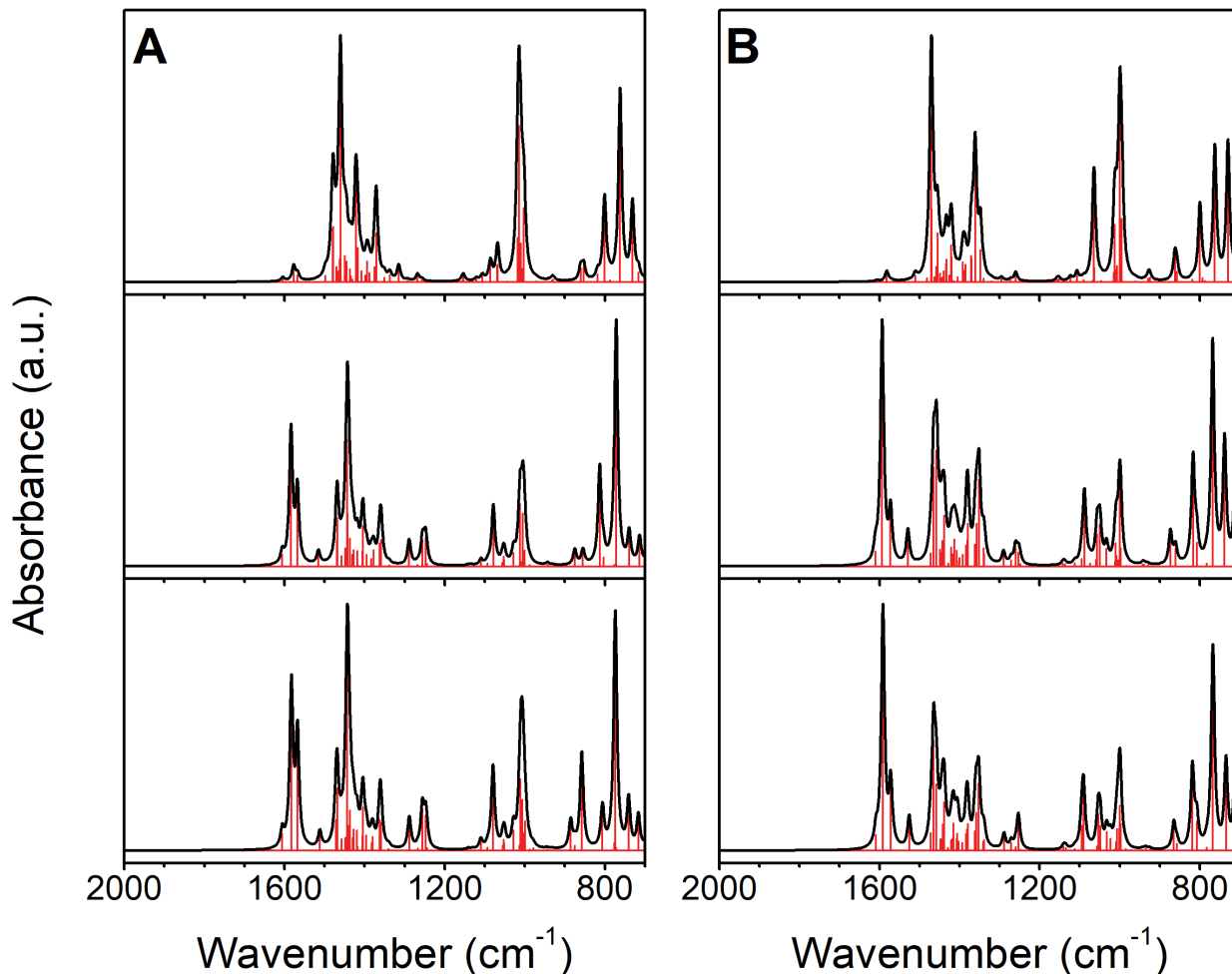


Figure S36. DFT calculated FTIR spectra of **C1** attached to Au in **A** the Cl down orientation using (Original Basis) (top), LAN (middle), and DEF (bottom) and **B** Cl up orientation using (Original Basis) (top), LAN (middle), and DEF (bottom).

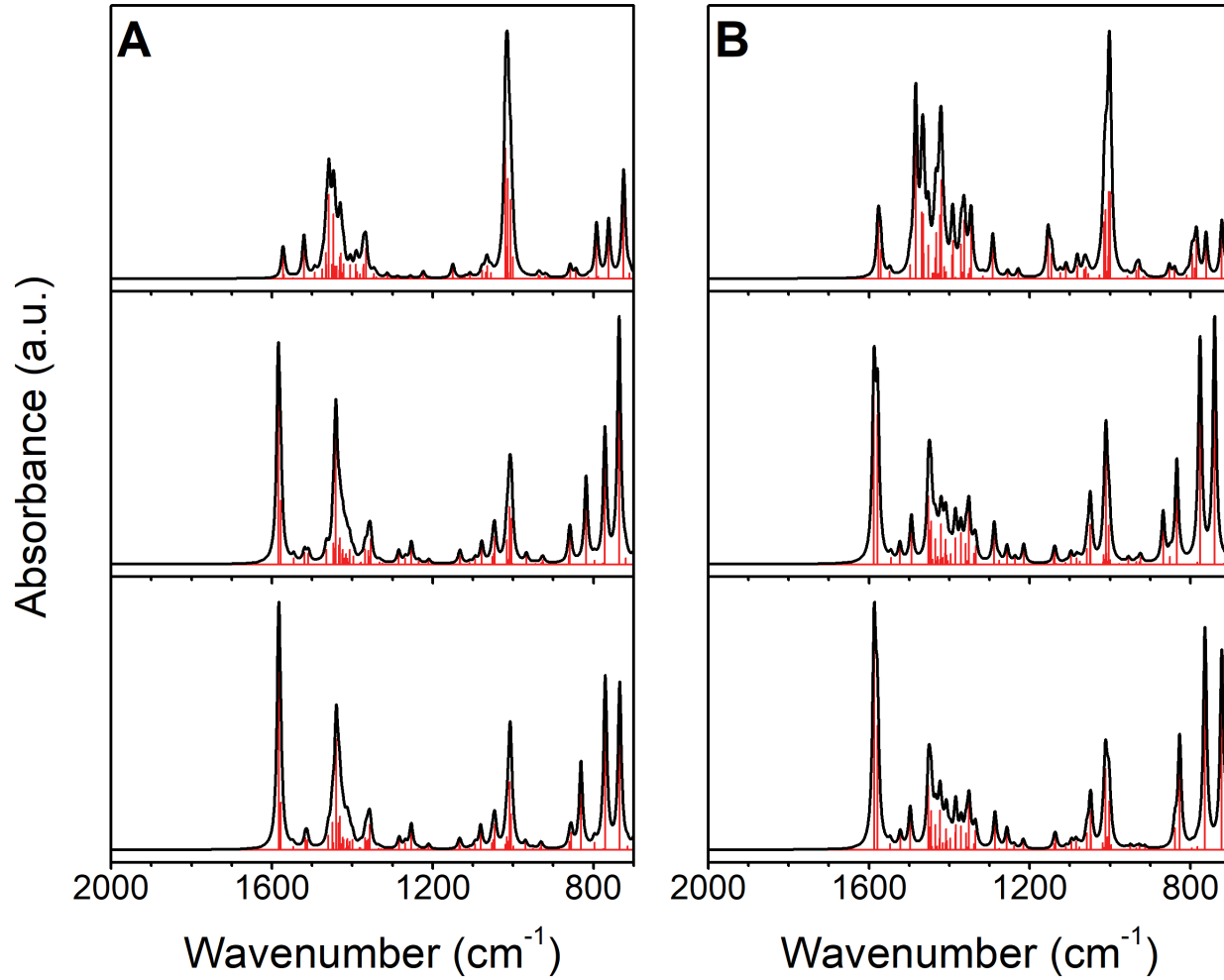


Figure S37. DFT calculated FTIR spectra of **C2** attached to Au in **A** the Cl down orientation using (Original Basis) (top), LAN (middle), and DEF (bottom) and **B** Cl up orientation using (Original Basis) (top), LAN (middle), and DEF (bottom).

DFT Optimized Structure Parameters

Table S5. Orientational and energetic parameters of the PBE D3 LANL2DZ DFT optimized structures of **C1m** and **C2m**.

Structure	Cl orientation	Tilt angles		Twist Angle Ψ_1	Relative Energy	S-Au (Å)
		θ_1	θ_2			
C1m	Up	71	14	92	2.75	2.32
	Down	73	48	265	0	2.32
C2m	Up	69	20	92	0	2.25
	Down	74	68	267	1.84	2.32

Table S6. Orientational and energetic parameters of the wB97XD LANL2DZ optimized structures of **C1m** and **C2m**.

Structure	Cl orientation	Tilt angles		Twist Angle Ψ_1	Relative Energy	S-Au (Å)
		θ_1	θ_2			
C1m	Up	74	75	91	0.72	2.34
	Down	76	23	268	0	2.40
C2m	Up	73	23	91	3.79	2.22
	Down	75	72	269	0	2.28

Relative Intensity and Transition Dipole Analysis with Computed Orientations

TDM analysis using Functional: PBE D3 Basis Set: LANL2DZ

Table S7. Experimentally determined TDM and the DFT (PBE-D3-LANL2DZ) calculated TDMs with respect to normal for orientation determination of the C1 monolayer on Au.

Peak PM	PM-IRRAS Area	Peak Calc	Calc Area	θ ($^{\circ}$) $\pm 6^{\circ}$	Calculated Peak Cl down	Relative Intensity	TDM angle at peak Cl down	Calculated Peak Cl up	Relative Intensity	TDM angle Cl up	Transition (DFT)
1596	0.0745	1597	0.12849	40	1604	1.2	57	1606	0.4	86	bipyridine breathing modes
					1577	4.6	22	1582	2.7	56	bipyridine breathing modes
1488	0.02344	1486	0.02757	23	1480	15.6	32	1481	1.0	79	C-H bending (bipyridine, Cp*)
					1478	16.4	86				C-H bending (bipyridine, Cp*)
1466	0.02734	1464	0.08584	56	1470	4.5	88	1471	41.8	12	C-H bending (Cp*)
					1465	58.9	89	1470	18.5	41	C-H bending (Cp*)
					1460	3.3	20	1458	4.0	72	C-H bending (Cp*)
					1449	7.8	10	1455	12.5	62	C-H bending (Cp*)
					1445	4.3	28				C-H bending (bipyridine, Cp*)
					1444	6.3	59	1432	5.8	29	C-H bending (bipyridine, Cp*)
1441	3.74E-02	1435	0.05767	36	1436	3.9	48	1433	4.8	67	C-H bending (Cp*)
					1422	28.5	10	1421	9.5	45	C-H bending (Cp*) Cp* breathing symmetric
					1417	10.2	26	1419	6.3	38	C-H bending (Cp*) Cp* breathing symmetric
1390	0.0343	1391	0.05497	38	1393	6.2	45	1392	5.0	33	C-H bending (Cp*) Cp* breathing asymmetric
1318	0.00252	1320	0.00953	59	1315	4.7	8	1321	0.3	77	C-H bending, C-C breathing mix (bipyridine)
1229	0.00703	1237	0.01077	36	N/A		N/A	N/A		N/A	N/A
1110	0.01121	1110	0.01266	20	1106	1.8	44	1107	2.2	32	asymmetric C-H bending, C-C breathing mix (bipyridine)
1075	0.00276	1074	0.02314	70	1068	5.1	85	1064	24.5	17	asymmetric C-H bending, C-C breathing mix (bipyridine)
					1067	5.3	89	1063	3.6	45	asymmetric C-H bending, C-C breathing mix (bipyridine)
1027	0.01348	1031	0.05263	60	1015	46.4	21	1012	14.6	36	C-H bending (Cp*)
944	7.51E-04	940	0.00132	41	1002	22.1	37	1000	40.5	24	symmetric C-H bending (Cp*), Cp* vibration mix
								862	6.9	42	out of plane C-H bending, bpy
839	0.00829	845	0.01142	32	853	4.6	39	857	2.7	88	out of plane C-H bending, bpy
818	0.00624	813	0.02673	61	818	2.3	14	818	0.7	90	bpy breathing both byps

Table S8. Experimentally determined TDM and the DFT (PBE-D3-LANL2DZ) calculated TDMs with respect to normal for orientation determination of the C2 monolayer on Au.

Peak PM-IRRAS	PM-IRRAS Area	Peak Calc	Calc Area	θ ($^{\circ}$) $\pm 6^{\circ}$	Calculated Peak Cl down	Relative Intensity	TDM angle at peak Cl down	Calculated Peak Cl up	Relative Intensity	TDM angle Cl up	Transition (DFT)
1589	0.02207	1587	0.09567	61	1572	12.2	50	1577	23.0	57	phenylpyridine breathing modes
					1569	1.8	9	1571	11.7	10	phenylpyridine breathing modes
1526	0.00693	1525	0.00703	7	1520	18.0	70	1548	3.0	61	phenylpyridine breathing mode
1476	6.04E-03	1465	0.03572	66	1475	4.3	68	1484	70.0	15	C-H bend (Cp^*) and Cp^* breathing
1448	4.84E-04	1451	0.03455	83	1465	11.2	16	1468	26.3	47	C-H bend (Cp^*)
					1464	6.0	47	1465	25.4	17	C-H bend (Cp^*)
					1458	36.4	38	1464	9.9	7	C-H bend (Cp^* , ppy)
					1451	6.3	75	1453	13.3	80	C-H bend (Cp^*)
					1446	27.8	25	1452	7.3	41	C-H bend (Cp^*)
					1443	5.4	49	1441	2.3	66	C-H bend (Cp^*)
					1439	5.4	51				C-H bend (Cp^*)
					1435	0.3	35				C-H bend (Cp^*)
1431	7.95E-04	1428	0.00693	70	1432	3.8	23	1434	8.2	42	C-H bend (Cp^* , phenylpyridine)
					1431	9.5	35	1433	18.1	15	C-H bend (Cp^* , phenylpyridine)
					1429	11.1	37	1427	2.1	80	C-H bend (Cp^* , phenylpyridine)
								1425	2.1	89	C-H bend (Cp^* , phenylpyridine)
								1423	25.2	32	C-H bend (Cp^* , phenylpyridine)
								1420	39.0	17	C-H bend (Cp^*)
1395	0.01445	1390	0.02209	36	1391	6.2	26	1393	9.4	23	Cp^* breathing, C-H bending (Cp^*)
					1388	3.0	44	1391	15.1	37	Cp^* breathing, C-H bending (Cp^*)
1370	1.34E-03	1371	0.00323	50	1380	2.1	82	1371	13.7	58	C-H bending symmetric (Cp^*)
								1346	21.1	28	C-H bending asymmetric (ppy)
1300	6.12E-04	1299	0.0046	69	1313	2.0	28	1316	1.1	90	C-H bending asymmetric (ppy), phenylpyridine breathing mix
								1292	17.0	19	C-H bending asymmetric (ppy)
1227	0.00115	1232	0.00284	50	1223	3.0	22	1255	2.7	44	C-H bending asymmetric (ppy)
1186	3.61E-04	1193	0.00187	64	N/A		N/A				C-H bending asymmetric (ppy, Cp^*)
1158	1.17E-03	1159	0.00535	62	1150	5.2	44	1154	17.6	21	C-H bending asymmetric (ppy, Cp^*)
1104	9.75E-03	1097	1.70E-02	41	1107	1.9	43	1110	5.1	17	C-H bending asymmetric (ppy)
1053	1.23E-03	1060	1.72E-02	74	1064	5.6	73	1065	3.6	47	Methyl wagging (Cp^*)
1028	7.03E-03	1031	0.04125	66	1019	56.1	24	1015	22.3	30	ppy breathing
					1013	43.2	83	1011	27.2	26	Methyl wagging (Cp^*), ppy breathing
								999	34.1	25	C-H bending asymmetric (ppy), pyridine breathing
912	4.41E-04	913	0.00539	73	937	1.6	39	935	3.4	2	Methyl Wagging asymmetric
					933	1.3	50	929	5.1	16	Methyl wagging (Cp^*) asymmetric

865	1.29E-03	870	0.00329	51	858	5.7	12	853	5.1	32	C-H bending ppy out of plane
845	0.00761	845	0.02136	53	844	3.5	70	840	3.7	68	C-H bending ppy out of plane
823	0.00314	838	0.01172	59							C-H bending ppy out of plane
815	5.20E-04	814	0.02141	81	813	0.9	63	809	1.5	66	pyridine and phenyl mixed breathing

TDM Analysis using Functional: wB97XD Basis Set: LANL2DZ

Table S9. Experimentally determined TDM and the DFT (wB97XD-LANL2DZ) calculated TDMs with respect to normal for orientation determination of the C1 monolayer on Au.

Peak PM	PM-IRRAS Area	Peak Calc	Calc Area	θ ($^{\circ}$) $\pm 6^{\circ}$	Calculated Peak Cl down (scaled by 0.9485)	Relative Intensity	TDM angle at peak Cl down	Calculated Peak Cl up (scaled by 0.9485)	Relative Intensity	TDM angle Cl up	Transition (DFT)
1596	0.0745	1597	0.12849	40	1605	4.8	45	1610	3.8	49	bipyridine breathing mode
					1584	54.9	20	1593	60.4	19	bipyridine breathing mode
					1568	30.2	32	1572	13.1	17	bipyridine breathing modes
					1515	5.4	28	1529	8.4	34	bipyridine breathing modes
1488	0.02344	1486	0.02757	23				1472	3.4	45	C-H bending (bipyridne, Cp*)
1466	0.02734	1464	0.08584	56	1469	10.8	43	1465	24.9	25	C-H bending (bipyridne, Cp*)
					1468	19.6	57	1457	29.0	21	C-H bending (Cp*)
					1458	4.3	74	1448	4.3	7	C-H bending (Cp*)
					1448	7.4	41				C-H bending (Cp*) Cp* breathing asymmetric
1441	3.74E-02	1435	0.05767	36	1443	51.3	19	1442	6.4	10	C-H bending (Cp*)
					1442	21.2	39	1438	12.7	75	C-H bending (Cp*)
					1437	11.4	40	1412	6.8	46	C-H bending (bipyridne, Cp*)
					1427	6.7	65	1407	4.0	53	C-H bending (Cp*)
					1418	6.3	73				C-H bending (bipyridne, Cp*)
					1405	6.3	21				C-H bending (Cp*)
					1404	16.6	40				C-H bending (Cp*) Cp* breathing symmetric
1390	0.0343	1391	0.05497	38	1395	4.8	86	1392	3.0	85	C-H bending (Cp*) Cp* breathing asymmetric
					1377	6.7	16	1383	5.2	62	C-H bending, C-C breathing mix (bipyridne)
					1362	9.6	79	1380	6.7	39	C-H bending (Cp*) Cp* breathing asymmetric
					1359	10.8	81	1380	10.8	65	C-H bending (Cp*) Cp* breathing asymmetric
								1361	5.5	67	C-H bending (Cp*) Cp* breathing asymmetric
								1358	10.8	38	C-H bending (Cp*) Cp* breathing asymmetric
								1351	21.7	28	C-H bending (Cp*) Cp* breathing asymmetric
								1339	4.6	74	C-H bending (Cp*) Cp* breathing asymmetric
								1338	3.0	57	C-H bending (Cp*) Cp* breathing asymmetric
1318	0.00252	1320	0.00953	59	1289	10.3	25	1290	3.3	27	C-H bending, C-C breathing mix (bipyridne)
1229	0.00703	1237	0.01077	36	1255	10.7	19	1260	4.6	16	C-H bending, C-C breathing mix (bipyridne)
					1248	11.6	19	1252	3.6	40	C-H bending, C-C breathing mix (bipyridne)
1110	0.01121	1110	0.01266	20	1109	2.4	38	1112	0.8	27	C-H bending, C-C breathing mix (bipyridne)

									1094	1.9	57	C-H bending, bpy breathing mix asymmetric
1075	0.00276	1074	0.02314	70	1078	24.4	9	1088	18.0	20	C-H bending, C-C breathing mix (bipyridine)	
								1074	0.8	34	C-H Methyl wagging	
								1056	8.0	24	C-H Methyl wagging	
1027	0.01348	1031	0.05263	60	1028	5.5	23	1050	10.5	24	C-H bending, C-C breathing mix (bipyridine)	
					1012	25.5	21	1033	4.5	21	C-H bending (bipyridine, Cp*)	
					1005	21.6	12	1010	5.9	66	C-H Methyl wagging	
					1002	5.1	60	1000	19.1	33	C-H Methyl wagging	
					1002	5.1	58				C-H Methyl wagging	
				60	1000	6.5	37				C-H Methyl wagging bpy breathing mic	
944	7.51E-04	940	0.00132	41	942	0.4	46	943	0.5	63	out of plane C-H bending, bpy	
					875	6.3	73	873	8.3	51	out of plane C-H bending, bpy	
839	0.00829	845	0.01142	32	855	6.2	47	817	26.3	22	out of plane C-H bending, bpy	
818	0.00624	813	0.02673	61	813	39.2	17	807	6.0	20	out of plane C-H bending, bpy	

Table S10. Experimentally determined TDM and the DFT (wB97XD LANL2DZ) calculated TDMs with respect to normal for orientation determination of the C2 monolayer on Au.

Peak PM	PM-IRRAS Area	Peak Simulated	Simulated Area	θ ($^{\circ}$) $\pm 6^{\circ}$	Calculated Peak Cl down (scaled by 0.9485)	Relative Intensity	TDM angle at peak Cl down	Calculated Peak Cl up (scaled by 0.9485)	Relative Intensity	TDM angle Cl up	Transition (DFT)
1589	0.02207	1587	0.09567	61	1582	75.3	27	1587	57.1	32	phenylpyridine breathing (pyridine)
					1578	24.9	29	1578	47.3	30	phenylpyridine breathing (phenyl)
1526	0.00693	1525	0.00703	7	1514	4.7	87	1523	5.7	83	phenylpyridine breathing
1476	6.04E-03	1465	0.03572	66	1510	4.3	82	1494	14.3	17	C-H bend (Cp*) and Cp* breathing
					1463	5.7	60	1452	21.5	36	C-H bend (Cp*) and Cp* breathing
1448	4.84E-04	1451	0.03455	83	1448	8.2	39	1449	10.8	45	C-H bending asymmetric (ppy), phenylpyridine breathing mix
1431	7.95E-04	1428	0.00693	70	1446	6.2	88	1445	13.6	8	C-H bending, C-C breathing mix (phenylpyridine)
					1440	50.5	31	1435	8.1	81	C-H bend (Cp*) and Cp* breathing
					1432	7.5	83	1431	1.1	43	C-H bending asymmetric (ppy), phenylpyridine breathing mix
					1429	10.3	29	1421	12.7	50	C-H bend (Cp*)
					1424	5.7	78	1409	7.9	51	C-H bending, C-C breathing mix (phenylpyridine)
					1405	5.7	58				C-H bend (Cp*)
1395	0.01445	1390	0.02209	36	1399	3.1	90	1397	3.3	88	C-H bend (Cp*)
								1385	8.4	22	C-H bend (Cp*)
								1384	5.6	81	C-H bend (Cp*)
1370	1.34E-03	1371	0.00323	50	1367	5.9	36	1371	9.9	32	C-H bending, C-C breathing mix (phenylpyridine)
					1360	5.4	87	1359	6.5	48	C-H bend (Cp*)
					1354	9.9	88	1351	16.4	41	C-H bend (Cp*)

								1334	5.8	65	C-H bend (Cp*)
1300	6.12E-04	1299	0.0046	69	1285	5.0	66	1288	12.7	53	C-H bending, C-C breathing mix (phenylpyridine)
1227	0.00115	1232	0.00284	50	1254	8.4	30	1256	5.4	38	C-H bending, C-C breathing mix (phenylpyridine)
1186	3.61E-04	1193	0.00187	64	1209	1.8	56	1215	6.1	32	C-H bending, C-C breathing mix (phenylpyridine)
1158	1.17E-03	1159	0.00535	62	1134	2.9	53	1140	1.8	31	C-H bending (Cp*, ppy), C-C breathing mix (Cp*)
1104	9.75E-03	1097	1.70E-02	41	1108	0.7	88	1097	3.3	4	C-H bending, C-C breathing mix (phenylpyridine)
					1095	2.1	24				C-H bending, C-C breathing mix (phenylpyridine)
1053	1.23E-03	1060	1.72E-02	74	1077	8.1	6	1057	5.0	27	Methyl Wagging asymmetric
					1051	3.1	68	1050	12.5	25	Methyl Wagging asymmetric
					1048	4.3	60	1048	8.9	18	C-H bending, C-C breathing mix (phenylpyridine)
					1046	10.7	26				Methyl Wagging asymmetric
1028	7.03E-03	1031	0.04125	66	1015	9.6	28	1017	0.8	64	Methyl Wagging asymmetric
					1008	22.2	35	1016	3.1	18	C-H bending (Cp*), C-C breathing mix (phenylpyridine)
					1002	17.8	19	1010	34.4	28	C-H bending (Cp*), C-C breathing mix (phenylpyridine)
								1003	12.3	29	Methyl Wagging asymmetric
912	4.41E-04	913	0.00539	73	926	1.7	38	924	2.1	69	out of plane C-H bending, ppy
865	1.29E-03	870	0.00329	51	862	11.6	62	868	15.8	38	out of plane C-H bending, ppy
845	0.00761	845	0.02136	53				851	2.4	54	out of plane C-H bending, ppy
823	0.00314	838	0.01172	59							out of plane C-H bending, ppy
815	5.20E-04	814	0.02141	81	811	33.0	15	834	32.1	14	out of plane C-H bending, ppy

TDM analysis using the wB97XD functional and the DEF2SVP basis set

Table S11. Experimentally determined TDM and the DFT (wB97XD functional and the DEF2SVP basis set) calculated TDMs with respect to normal for orientation determination of the C1 monolayer on Au used in final determination of the orientation of C1m on the surface.

Peak PM	PM-IRRAS Area	Peak Calc	Calc Area	$\theta (^{\circ}) \pm 6^{\circ}$	Calculated Peak Cl down (scaled by 0.9485)	Relative Intensity	TDM angle at peak Cl down	Calculated Peak Cl up (scaled by 0.9485)	Relative Intensity	TDM angle Cl up	Transition (DFT)
1596	0.0745	1597	0.12849	40	1605	5.9	48	1609	4.6	50	bipyridine breathing modes
					1583	56.7	20	1591	69.2	16	bipyridine breathing modes
					1567	39.4	32	1572	18.5	17	bipyridine breathing modes
					1512	5.7	29	1526	9.1	34	bipyridine breathing modes
1488	0.02344	1486	0.02757	23	1471	10.9	63	1472	5.1	40	C-H bending (bipyridine, Cp*)
1466	0.02734	1464	0.08584	56	1468	21.8	42				C-H bending (bipyridine, Cp*)
					1443	66.1	18	1465	31.8	16	C-H bending (Cp*)
					1441	8.8	46	1458	19.0	33	C-H bending (Cp*)
								1442	7.7	6	C-H bending (bipyridine, Cp*)
								1438	14.0	70	C-H bending (Cp*)
1441	3.74E-02	1435	0.05767	36	1436	14.0	39				C-H bending (bipyridine, Cp*)
					1427	7.5	62	1415	7.9	48	C-H bending (Cp*)
					1419	7.2	80				C-H bending (bipyridine, Cp*)
1390	0.0343	1391	0.05497	38	1406	5.4	54	1384	4.8	83	C-H bending (Cp*) Cp* breathing asymmetric
					1404	15.2	30	1381	6.1	52	C-H bending (Cp*) Cp* breathing symmetric
					1396	5.3	84				C-H bending (Cp*) Cp* breathing symmetric
								1379	7.8	49	C-H bending, C-C breathing mix (bipyridine)
1318	0.00252	1320	0.00953	59	1362	10.6	75	1361	5.6	64	C-H bending (Cp*) Cp* breathing symmetric
					1359	9.8	80	1358	11.0	37	C-H bending (Cp*) Cp* breathing asymmetric
								1352	19.3	31	C-H bending (Cp*) Cp* breathing asymmetric
1229	0.00703	1237	0.01077	36	1288	11.1	25	1253	9.8	29	C-H bending, C-C breathing mix (bipyridine)
					1256	14.5	18				C-H bending, C-C breathing mix (bipyridine)
					1247	12.2	20				C-H bending, C-C breathing mix (bipyridine)
1110	0.01121	1110	0.01266	20	1110	3.3	37	1095	7.2	30	asymmetric C-H bending, C-C breathing mix (bipyridine)
								1090	17.0	16	asymmetric C-H bending, C-C breathing mix (bipyridine)
1075	0.00276	1074	0.02314	70	1079	28.9	14	1053	10.4	19	asymmetric C-H bending (Cp*, bpy), C-C breathing mix (bipyridine)
								1048	7.2	30	asymmetric C-H bending (Cp*, bpy), C-C breathing mix (bipyridine)
1027	0.01348	1031	0.05263	60	1028	7.0	27	1032	5.5	15	asymmetric C-H bending, C-C breathing mix (bipyridine)
					1011	24.7	20	1007	6.2	45	C-H bending (Cp*) Cp* and bpy breathing asymmetric
					1009	7.3	35	1000	6.4	30	C-H bending (Cp*) Cp* and bpy breathing asymmetric

					1006	5.9	24	1000	13.0	37	C-H bending (Cp^*) Cp^* and bpy breathing asymmetric
					1005	56.7	25				C-H bending (Cp^*) Cp^* and bpy breathing asymmetric
					1003	39.4	76				C-H bending (Cp^*) Cp^* and bpy breathing asymmetric
944	7.51E-04	940	0.00132	41	999	5.7	33	998	7.8	9	out of plane C-H bending bpy, bpy breathing mix
					885	10.9	65	865	7.7	47	out of plane C-H bending, bpy
839	0.00829	845	0.01142	32	858	21.8	16	818	23.5	21	out of plane C-H bending, bpy
818	0.00624	813	0.02673	61	806	66.1	22	808	8.4	17	out of plane C-H bending, bpy, bpy breathing mix

Table S12. Experimentally determined TDM and the DFT (wB97XD functional and the DEF2SVP basis set) calculated TDMs with respect to normal for orientation determination of the **C2** monolayer on Au used in final determination of the orientation of C2m on the surface.

Peak PM	PM-IRRAS Area	Peak Calc	Calc Area	θ ($^\circ$) $\pm 6^\circ$	Calculated Peak Cl down (scaled by 0.9485)	Relative Intensity	TDM angle at peak Cl down	Calculated Peak Cl up (scaled by 0.9485)	Relative Intensity	TDM angle Cl up	Transition (DFT)
1589	0.02207	1587	0.09567	61	1581	88.2	27	1587	68.7	31	phenylpyridine breathing modes
					1578	13.9	37	1579	40.6	36	phenylpyridine breathing modes
					1513	4.7	85				phenylpyridine breathing mode
1526	0.00693	1525	0.00703	7	1512	3.9	76	1522	5.0	78	C-H bend (Cp^*) and Cp^* breathing asymmetric
1476	6.04E-03	1465	0.03572	66	1460	5.6	45	1497	13.2	16	C-H bend (Cp^*) and Cp^* breathing asymmetric
1448	4.84E-04	1451	0.03455	83	1449	10.6	44	1452	20.9	37	C-H bend (Cp^*) and Cp^* breathing asymmetric
					1440	42.7	32	1449	7.5	50	C-H bend (Cp^*) and Cp^* breathing asymmetric
					1432	10.3	75	1445	12.8	5	C-H bend (Cp^*)
1431	7.95E-04	1428	0.00693	70	1430	12.9	21	1434	8.3	90	C-H bend (Cp^*)
					1424	4.9	84	1423	12.9	59	C-H bend (Cp^* , phenylpyridine)
					1414	3.7	42	1408	6.8	59	C-H bend (Cp^*)
1395	0.01445	1390	0.02209	36	1412	4.4	72	1397	3.8	88	C-H bend (Cp^*)
1370	1.34E-03	1371	0.00323	50	1367	4.7	38	1384	5.8	46	C-H bend (Cp^* , phenylpyridine)
					1360	4.1	80	1384	8.2	44	phenylpyridine bending
					1355	9.9	88	1370	7.7	35	C-H bend (Cp^* , phenylpyridine)
								1358	5.5	55	C-H bend (Cp^*)
								1351	15.1	38	C-H bend (Cp^*)
								1334	6.3	66	C-H bending asymmetric (ppy)
1300	6.12E-04	1299	0.0046	69	1284	4.4	66	1286	11.8	54	C-H bending asymmetric (ppy), phenylpyridine breathing mix
1227	0.00115	1232	0.00284	50	1252	9.7	29	1257	6.8	38	Methyl wagging (Cp^*)
1186	3.61E-04	1193	0.00187	64	1209	2.0	19	1216	3.2	40	Methyl wagging (Cp^*)
1158	1.17E-03	1159	0.00535	62	1134	2.8	50	1136	3.9	51	C-H bending asymmetric (ppy), phenylpyridine breathing mix
1104	9.75E-03	1097	1.70E-02	41	1077	8.8	4	1096	2.6	11	C-H bending asymmetric (ppy), phenylpyridine breathing mix
1053	1.23E-03	1060	1.72E-02	74	1049	3.9	75	1058	5.5	23	Methyl wagging (Cp^*)
					1045	10.1	24	1049	12.7	26	Methyl wagging (Cp^*)

								1047	4.9	15	C-H bend (Cp*)
1028	7.03E-03	1031	0.04125	66	1017	2.2	34	1011	26.4	30	Methyl wagging (Cp*)
					1014	5.0	15	1007	4.3	14	C-H bending asymmetric (ppy), phenylpyridine breathing mix
					1008	26.2	23	1002	15.9	26	C-H bending asymmetric (ppy), phenylpyridine breathing mix
912	4.41E-04	913	0.00539	73	1004	7.7	88	927	1.2	65	C-H bending asymmetric (ppy), phenylpyridine breathing mix
					1003	13.8	17				C-H bending asymmetric (ppy), phenylpyridine breathing mix
865	1.29E-03	870	0.00329	51	857	6.8	77	840	0.2	69	C-H bending ppy out of plane
845	0.00761	845	0.02136	53	850	33.1	13	839	7.2	72	C-H bending ppy out of plane
823	0.00314	838	0.01172	59	797	2.9	17	827	36.1	11	C-H bending Cp* out of plane
815	5.20E-04	814	0.02141	81	771	41.0	34	796	0.6	42	C-H bending ppy out of plane

Visualizations of select IR modes

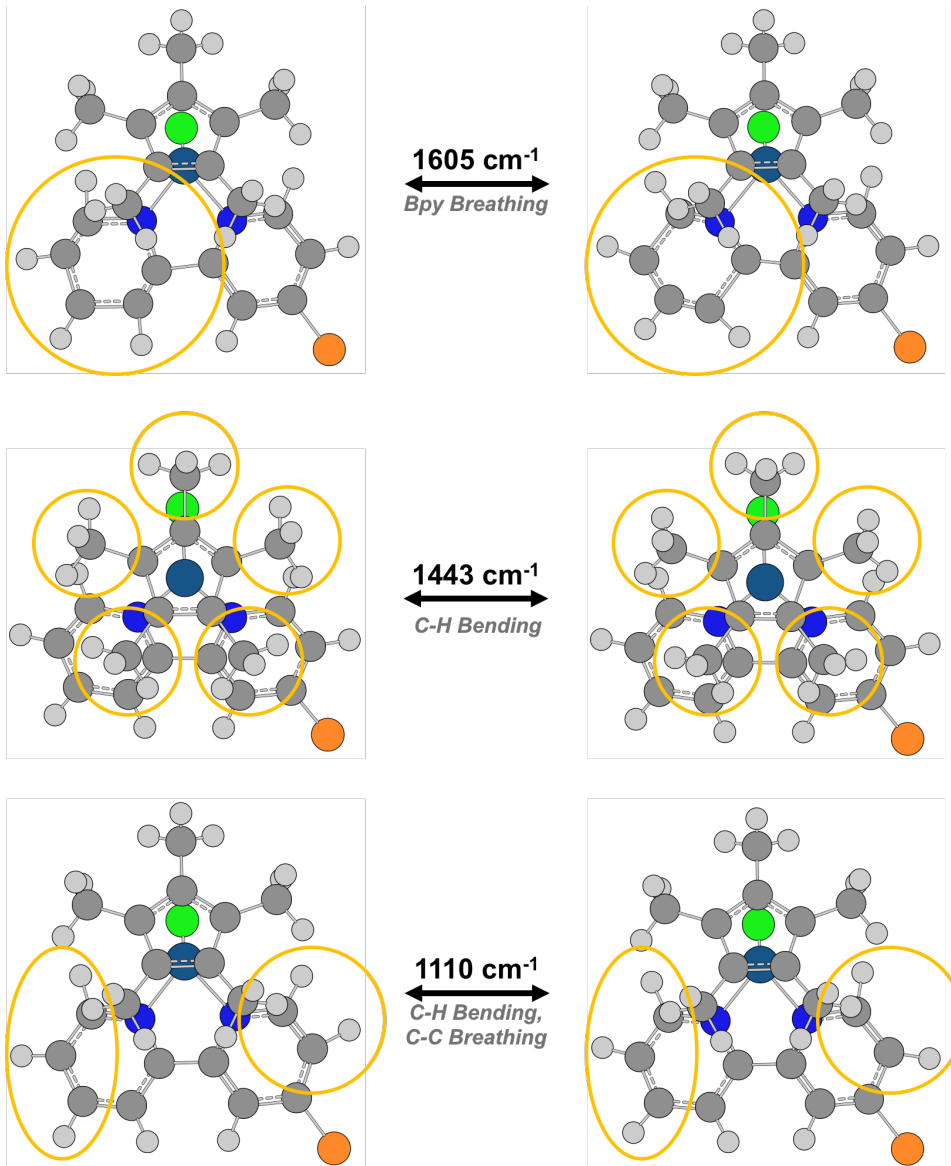


Figure S38. Visualization of displacements along key normal modes for **C1m** in the Cl down orientation (wB97XD functional and the DEF2SVP basis set with a 0.9485 scaling factor). Each mode is labeled with the corresponding vibrational frequency and a description; yellow circles are used to highlight areas of the molecule that have the largest displacements. All normal modes are reported in **Table S11**. Au atoms have been removed from the molecular structures for clarity.

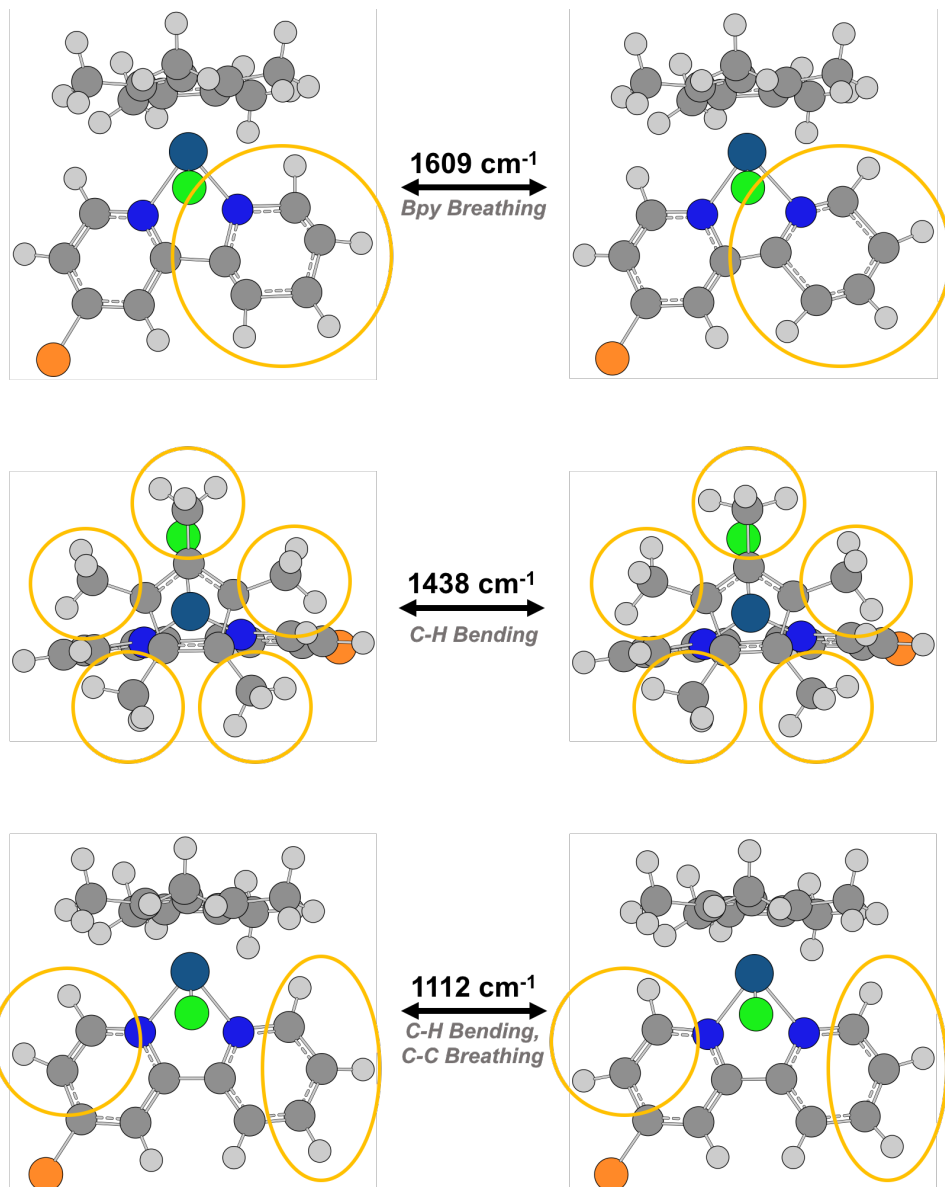


Figure S39. Visualization of displacements along key normal modes for **C1m** in the Cl up orientation (wB97XD functional and the DEF2SVP basis set with a 0.9485 scaling factor). Each mode is labeled with the corresponding vibrational frequency and a description; yellow circles are used to highlight areas of the molecule that have the largest displacements. All normal modes are reported in **Table S11**. Au atoms have been removed from the molecular structures for clarity.

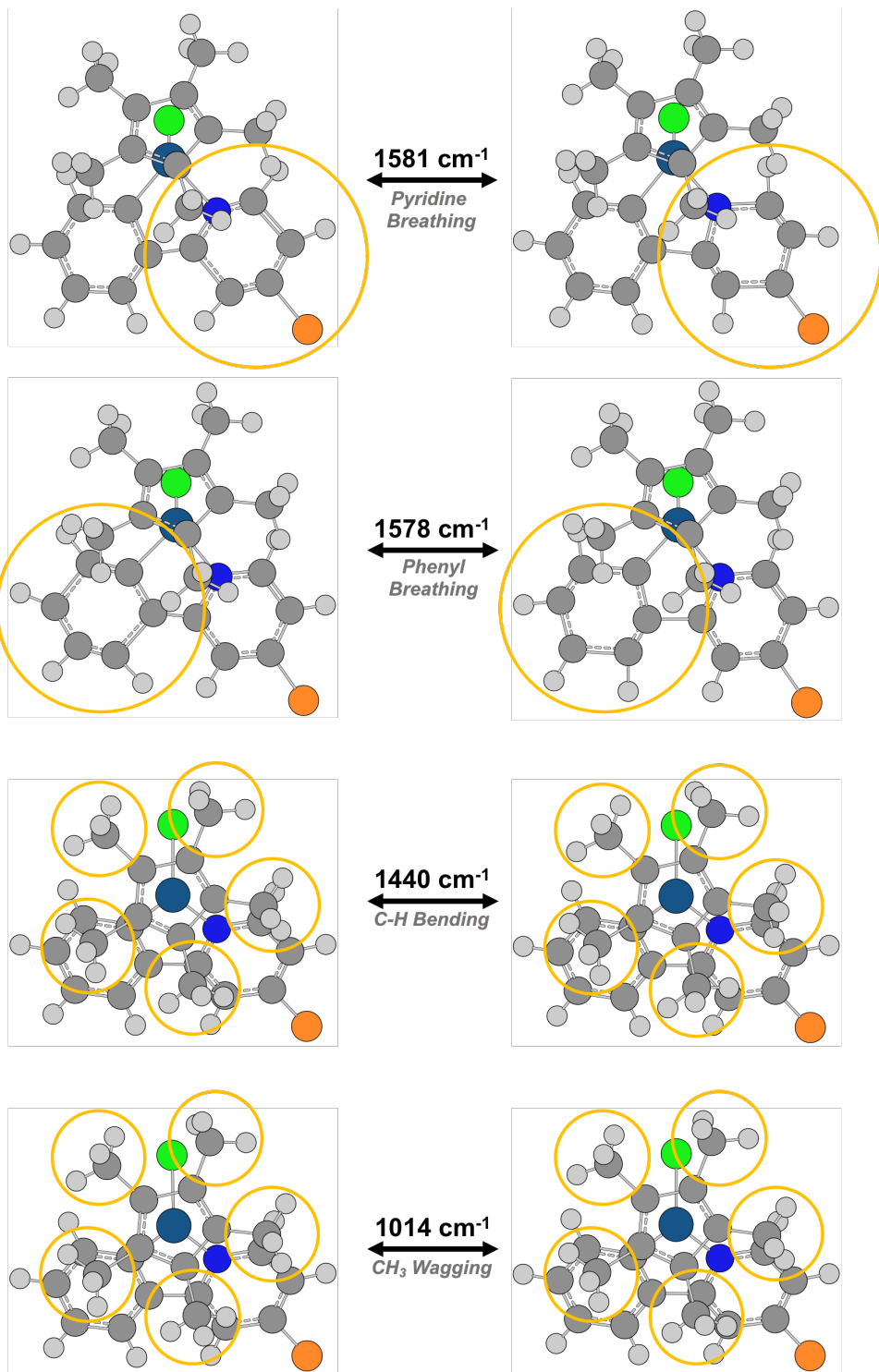


Figure S40. Visualization of displacements along key normal modes for **C2m** in the Cl down orientation (wB97XD functional and the DEF2SVP basis set with a 0.9485 scaling factor). Each mode is labeled with the corresponding vibrational frequency and a description; yellow circles are used to highlight areas of the molecule that have the largest displacements. All normal modes are reported in **Table S12**. Au atoms have been removed from the molecular structures for clarity.

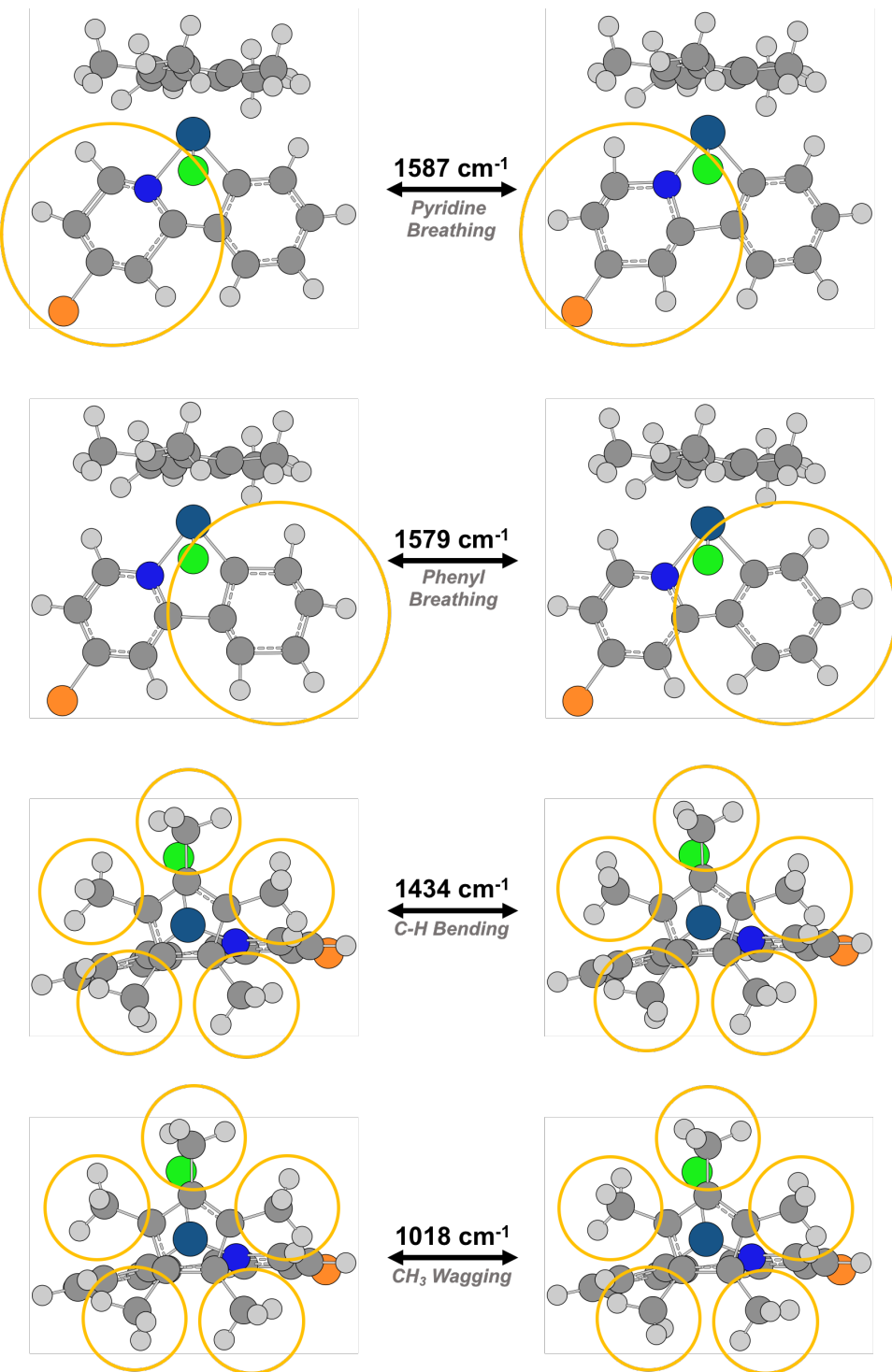


Figure S41. Visualization of displacements along key normal modes for **C2m** in the Cl up orientation (wB97XD functional and the DEF2SVP basis set with a 0.9485 scaling factor). Each mode is labeled with the corresponding vibrational frequency and a description; yellow circles are used to highlight areas of the molecule that have the largest displacements. All normal modes are reported in **Table S12**. Au atoms have been removed from the molecular structures for clarity.

Crystallographic Data

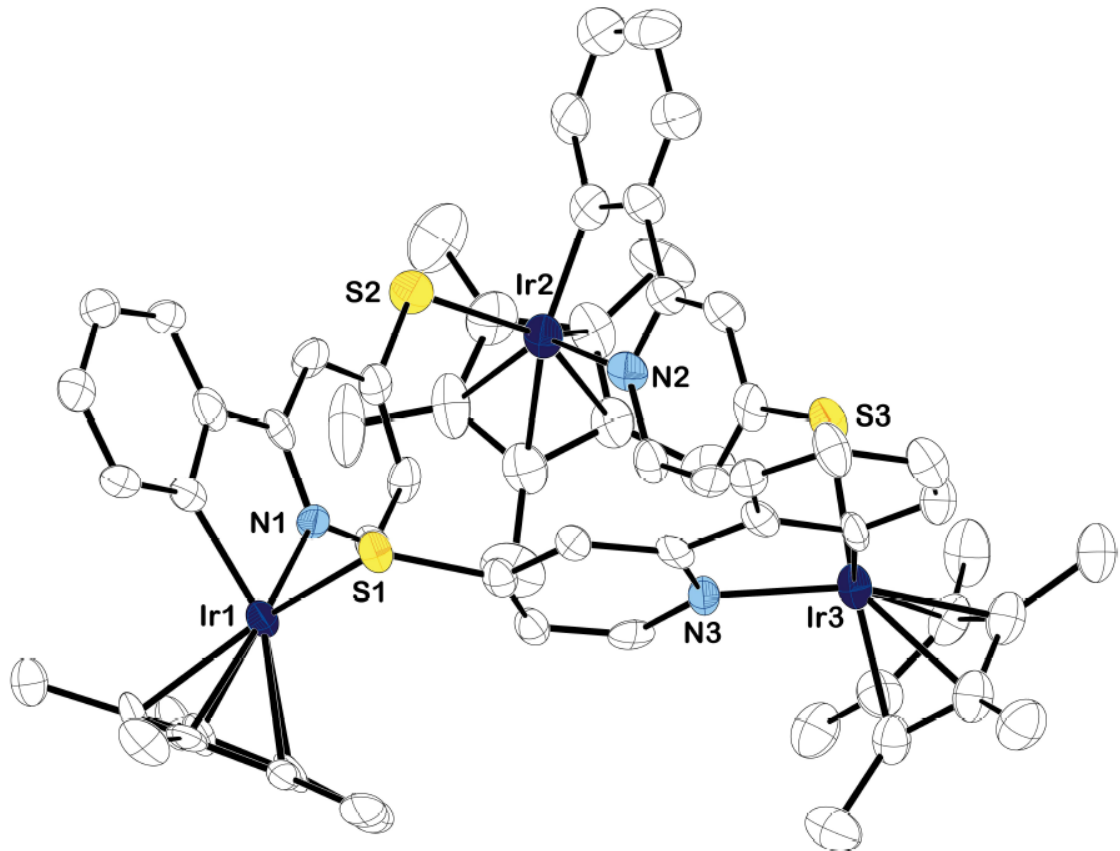


Figure S42. Solid-state structure of $[\text{Cp}^*\text{Ir}(2\text{-phenylpyridine-4-thiol})]_3$ (**C3**) as determined by single-crystal X-ray diffraction. Thermal ellipsoids are set at the 50% probability level. Non-coordinating ortho-dichlorobenzene molecules and carbon bound hydrogens were omitted for clarity.

Table S13. Crystal data and structure refinement for complex **C3**

Empirical Formula	C _{85.66} H _{81.11} Cl _{7.46} Ir ₃ N ₃ S ₃
Formula weight	2089.84
Temperature/K	100.0
Crystal system	monoclinic
Space group	C2/c
a/Å	45.563(8)
b/Å	18.693(3)
c/Å	21.023(4)
$\alpha/^\circ$	90
$\beta/^\circ$	90.978(4)
$\gamma/^\circ$	90

Volume/ Å ³	17902(5)
Z	8
ρcalcg/cm ³	1.551
μ/mm 1	4.784
F(000)	8175.0
Crystal size/mm3	0.3 × 0.1 × 0.1
Radiation	MoKα ($\lambda = 0.71073$)
2θ range for data collection/°	3.04 to 48.828
Index Ranges	-52 ≤ h ≤ 52, -21 ≤ k ≤ 21, -24 ≤ l ≤ 24
Reflections Collected	104645
Independent reflections	14729 [Rint = 0.1623, Rsigma = 0.1008]
Data/restraints/parameters	14729/72/955
Goodness-of-fit on F2	1.027
Final R indexes [I>=2s (I)]	R ₁ = 0.0491, wR ₂ = 0.1018
Final R indexes [all data]	R ₁ = 0.0910, wR ₂ = 0.116
Largest diff. peak/hole / e Å ⁻³	2.33/-1.19

Notes on refinement. For highly disordered ortho-dichlorobenzene molecules, the PLATON routine SQUEEZE was used to account for the corresponding electrons as a diffuse contribution to the overall scattering without specific atom positions.

X-ray Photoelectron Spectroscopy **C1m**

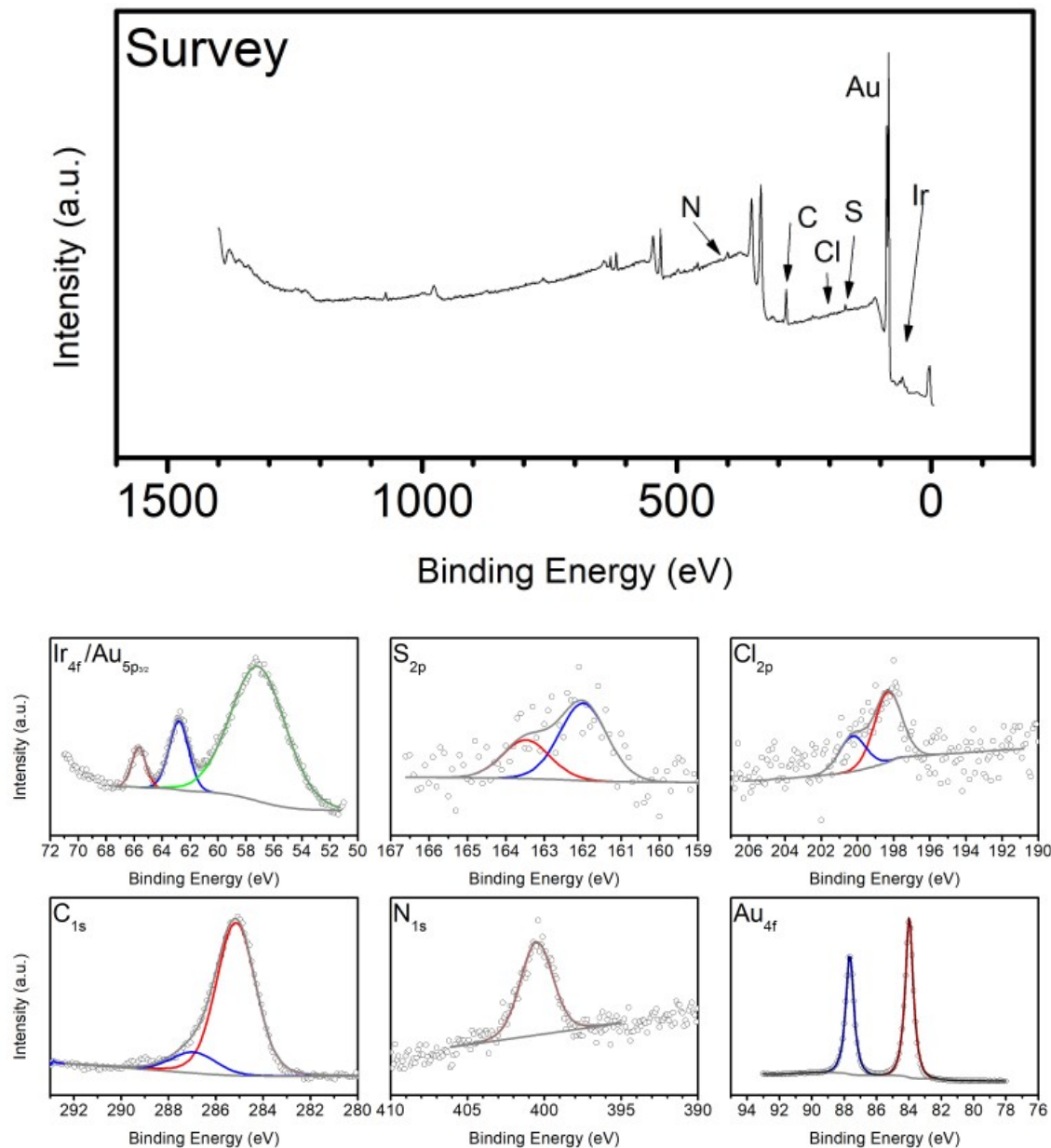


Figure S43. Survey (top) and high-resolution XPS of the **C1m** monolayer on Au. XPS peak positions of relevant elements (in eV) Ir (65.6, 62.7) S (163.5, 162.0), Cl (200.3, 198.3).

C2m

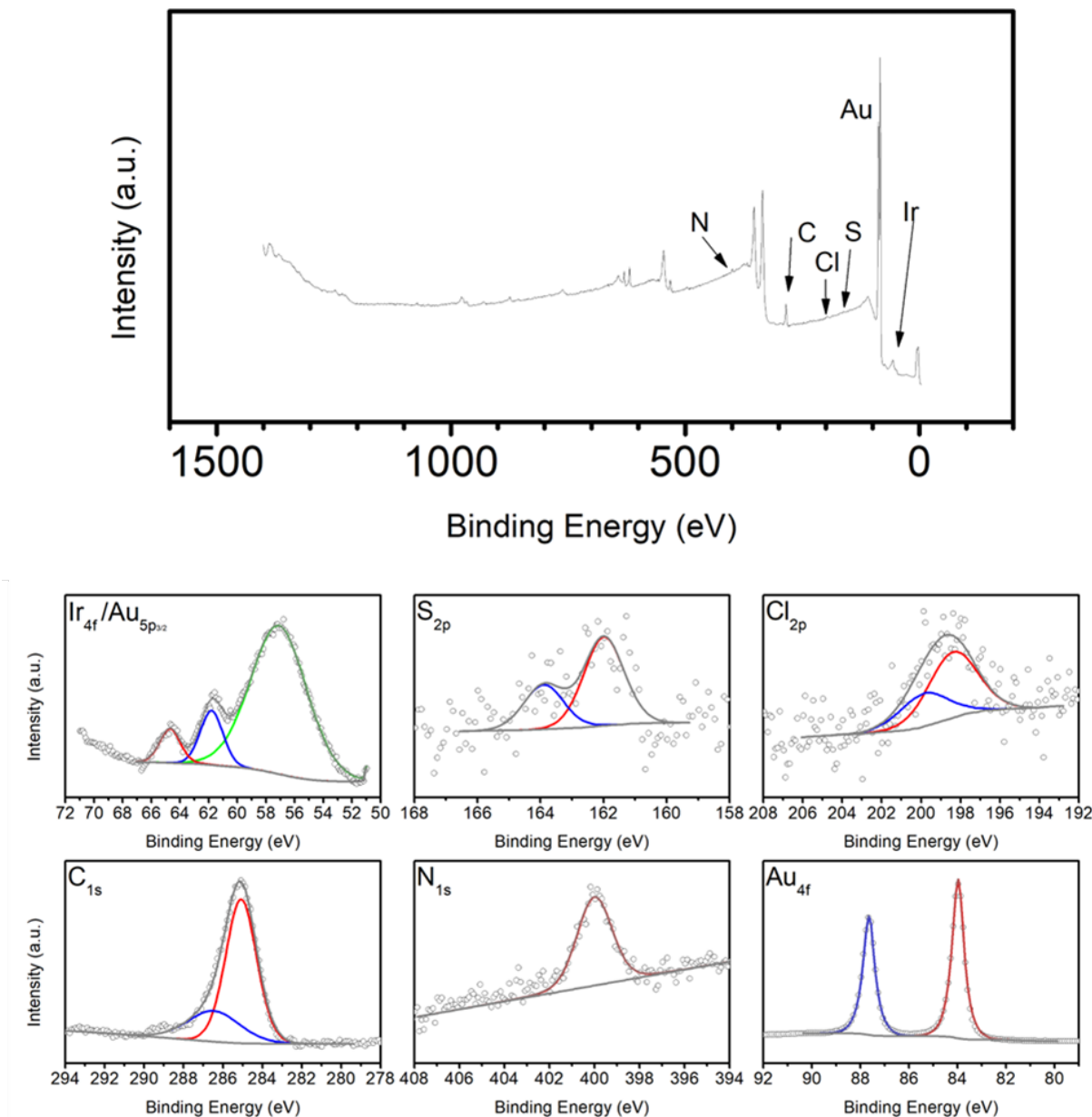


Figure S44. Survey (top) and high-resolution XPS of the **C2m** monolayer on Au. XPS peak positions of relevant elements (in eV) Ir (64.7, 61.8) S (163.9, 162.0), Cl (199.9, 198.4).

Quantification of Cl and Ir for C1m

Element	Peak	% Concentration	Ratio
Ir	4f _{7/2}	19.82	1 Ir : 2.55 Cl
Ir	4f _{5/2}	8.27	
Cl	2p _{3/2}	47.94	
Cl	2p _{1/2}	23.96	

The peaks of the high-resolution Ir 4f spectra for both **C1m** and **C2m** correspond to Ir being in the 3+ state. While there is overlap from Au 5d, there appears to be no lower energy Ir 4f signals, indicating that there is only Ir(III) with no Ir(I).

We believe the counter ion of **C1m** is serving as charge stabilization by ionic interactions similar to published reports.³⁰⁻³² Using the fitting analysis in CasaXPS and correcting for the relative sensitivity factors for each element, it was determined that there is about 1 Ir atom per 2.55 Cl. This demonstrates that the C1m monolayer co-packs with the Cl anion to balance the charges on the surface.

DFT Optimized xyz coordinates (Functional: wB97XD Basis Set: DEF2SVP)

DFT optimized xyz coordinates for C1m Cl down

Au	0.000000	0.000000	0.000000
Au	2.899130	0.000000	0.000000
Au	5.798270	0.000000	0.000000
Au	1.449570	2.510720	0.000000
Au	4.348700	2.510720	0.000000
Au	7.247830	2.510720	0.000000
Au	2.899130	5.021450	0.000000
Au	5.798270	5.021450	0.000000
Au	8.697400	5.021450	0.000000
Au	4.348700	7.532170	0.000000
Au	7.247830	7.532170	0.000000
Au	10.146970	7.532170	0.000000
Au	5.798270	10.042890	0.000000
Au	8.697400	10.042890	0.000000
Au	11.596530	10.042890	0.000000
Au	7.247830	12.553620	0.000000
Au	10.146970	12.553620	0.000000
Au	13.046100	12.553620	0.000000
Au	8.697400	0.000000	0.000000
Au	11.596530	0.000000	0.000000
Au	14.495670	0.000000	0.000000
Au	10.146970	2.510720	0.000000
Au	13.046100	2.510720	0.000000
Au	15.945230	2.510720	0.000000
Au	11.596530	5.021450	0.000000
Au	14.495670	5.021450	0.000000
Au	17.394800	5.021450	0.000000
Au	13.046100	7.532170	0.000000
Au	15.945230	7.532170	0.000000
Au	18.844370	7.532170	0.000000
Au	14.495670	10.042890	0.000000
Au	17.394800	10.042890	0.000000
Au	20.293930	10.042890	0.000000
Au	15.945230	12.553620	0.000000
Au	18.844370	12.553620	0.000000
N	9.900853	6.215612	3.592690
C	11.122938	6.730078	3.400877
C	12.213626	5.945674	3.070621
C	12.059978	4.554474	2.914799
C	10.755409	4.044077	3.076454
C	9.708449	4.889198	3.390091

N	7.429833	5.490019	3.693331
C	6.111406	5.294061	3.582057
C	5.579468	4.040290	3.315948
C	6.449962	2.966172	3.168039
C	7.821979	3.190028	3.205946
C	8.289399	4.476770	3.444601
H	11.210066	7.805750	3.508481
H	13.183262	6.405110	2.916384
H	10.587599	2.985196	2.917695
H	5.487784	6.171083	3.713760
H	4.507302	3.916911	3.218556
H	6.066710	1.969158	2.976539
H	8.514065	2.377114	3.022564
Ir	8.327418	7.177412	4.628666
C	7.915806	8.820565	6.024898
C	9.275338	8.376316	6.153120
C	7.041678	7.713292	6.284400
C	9.243388	6.983007	6.574953
C	7.874375	6.576236	6.651268
C	7.488445	10.203499	5.657618
H	7.394111	10.799403	6.571362
H	8.215261	10.682704	5.000730
H	6.528601	10.200443	5.140475
C	5.545110	7.758163	6.306736
H	5.187062	8.140028	7.267785
H	5.160942	8.406513	5.516328
H	5.117710	6.763041	6.164924
C	7.366085	5.230164	7.061906
H	7.108577	5.236088	8.125288
H	6.469885	4.956470	6.500046
H	8.114513	4.452965	6.897202
C	10.442719	6.146328	6.891166
H	10.759057	6.322161	7.923680
H	10.230543	5.081897	6.776007
H	11.281514	6.389742	6.235166
C	10.495266	9.234540	6.018434
H	10.668028	9.799683	6.939550
H	11.385060	8.630971	5.827633
H	10.386274	9.945496	5.196366
S	13.392888	3.535120	2.465137
Cl	7.748529	8.562903	2.776448

DFT optimized xyz coordinates for C1m Cl up

Au	0.000000	0.000000	0.000000
Au	2.899130	0.000000	0.000000
Au	5.798270	0.000000	0.000000
Au	1.449570	2.510720	0.000000
Au	4.348700	2.510720	0.000000
Au	7.247830	2.510720	0.000000
Au	2.899130	5.021450	0.000000
Au	5.798270	5.021450	0.000000
Au	8.697400	5.021450	0.000000
Au	4.348700	7.532170	0.000000
Au	7.247830	7.532170	0.000000
Au	10.146970	7.532170	0.000000
Au	5.798270	10.042890	0.000000
Au	8.697400	10.042890	0.000000
Au	11.596530	10.042890	0.000000
Au	7.247830	12.553620	0.000000
Au	10.146970	12.553620	0.000000
Au	13.046100	12.553620	0.000000
Au	8.697400	0.000000	0.000000
Au	11.596530	0.000000	0.000000
Au	14.495670	0.000000	0.000000
Au	10.146970	2.510720	0.000000
Au	13.046100	2.510720	0.000000
Au	15.945230	2.510720	0.000000
Au	11.596530	5.021450	0.000000
Au	14.495670	5.021450	0.000000
Au	17.394800	5.021450	0.000000
Au	13.046100	7.532170	0.000000
Au	15.945230	7.532170	0.000000
Au	18.844370	7.532170	0.000000
Au	14.495670	10.042890	0.000000
Au	17.394800	10.042890	0.000000
Au	20.293930	10.042890	0.000000
Au	15.945230	12.553620	0.000000
Au	18.844370	12.553620	0.000000
N	11.106891	5.782025	3.811725
C	12.422269	6.007819	3.701813
C	12.943560	7.204219	3.243008
C	12.073554	8.255525	2.916042
C	10.697248	7.997213	3.019970
C	10.247994	6.758690	3.441603
N	8.609884	5.078816	3.800150

C	7.369962	4.579656	3.732701
C	6.275723	5.360756	3.399357
C	6.477859	6.714488	3.156029
C	7.770866	7.220071	3.164604
C	8.828007	6.369409	3.467929
H	13.074861	5.198750	4.004161
H	14.016472	7.329589	3.156418
H	9.996995	8.784185	2.769895
H	7.262423	3.530231	3.975109
H	5.288248	4.917162	3.353021
H	5.641281	7.366439	2.930802
H	7.950911	8.266313	2.950206
Ir	10.213237	4.177825	4.882094
C	10.656477	2.805846	6.535718
C	11.790110	2.918619	5.670231
C	9.538095	2.326282	5.771684
C	11.392165	2.436864	4.360936
C	10.010958	2.068128	4.424561
C	10.640118	3.131973	7.991881
H	10.865552	2.220457	8.556077
H	11.384544	3.889710	8.237528
H	9.667028	3.509843	8.305795
C	8.182999	2.022667	6.332383
H	8.208089	1.089755	6.903800
H	7.847512	2.823652	6.994596
H	7.436900	1.903751	5.544055
C	9.220861	1.482327	3.298919
H	9.686996	0.557611	2.945398
H	8.194934	1.249617	3.589460
H	9.177552	2.167257	2.447556
C	12.289248	2.253307	3.188578
H	12.843197	1.311926	3.266632
H	11.699137	2.216172	2.273544
H	13.015128	3.064831	3.087784
C	13.170898	3.319104	6.090346
H	13.623786	2.529086	6.697095
H	13.819758	3.475606	5.225737
H	13.155606	4.237601	6.681498
S	12.646975	9.821427	2.389286
Cl	9.679590	5.915734	6.476631

DFT optimized xyz coordinates for C2m Cl down

Au	0.000000	0.000000	0.000000
Au	2.899130	0.000000	0.000000

Au	5.798270	0.000000	0.000000
Au	1.449570	2.510720	0.000000
Au	4.348700	2.510720	0.000000
Au	7.247830	2.510720	0.000000
Au	2.899130	5.021450	0.000000
Au	5.798270	5.021450	0.000000
Au	8.697400	5.021450	0.000000
Au	4.348700	7.532170	0.000000
Au	7.247830	7.532170	0.000000
Au	10.146970	7.532170	0.000000
Au	5.798270	10.042890	0.000000
Au	8.697400	10.042890	0.000000
Au	11.596530	10.042890	0.000000
Au	7.247830	12.553620	0.000000
Au	10.146970	12.553620	0.000000
Au	13.046100	12.553620	0.000000
Au	8.697400	0.000000	0.000000
Au	11.596530	0.000000	0.000000
Au	14.495670	0.000000	0.000000
Au	10.146970	2.510720	0.000000
Au	13.046100	2.510720	0.000000
Au	15.945230	2.510720	0.000000
Au	11.596530	5.021450	0.000000
Au	14.495670	5.021450	0.000000
Au	17.394800	5.021450	0.000000
Au	13.046100	7.532170	0.000000
Au	15.945230	7.532170	0.000000
Au	18.844370	7.532170	0.000000
Au	14.495670	10.042890	0.000000
Au	17.394800	10.042890	0.000000
Au	20.293930	10.042890	0.000000
Au	15.945230	12.553620	0.000000
Au	18.844370	12.553620	0.000000
N	9.879440	6.138434	3.561834
C	11.084043	6.700945	3.393562
C	12.205520	5.968772	3.048210
C	12.088971	4.579716	2.857876
C	10.817967	4.012665	3.015620
C	9.722590	4.807169	3.336781
C	6.038483	5.136097	3.487381
C	5.602200	3.842402	3.210711
C	6.521590	2.799062	3.070786
C	7.884554	3.072221	3.127288
C	8.319381	4.376409	3.381134
H	11.129807	7.776038	3.530096

H	13.159747	6.463995	2.910404
H	10.689453	2.948769	2.850636
H	5.310594	5.934294	3.607126
H	4.538911	3.639662	3.112615
H	6.175166	1.785103	2.895830
H	8.596983	2.267460	2.966967
Ir	8.229909	7.070117	4.482644
C	8.234567	8.834542	5.940402
C	9.275464	7.964767	6.298075
C	6.978268	8.080461	5.940974
C	8.701417	6.635685	6.521637
C	7.269243	6.755460	6.401765
C	8.333440	10.281668	5.576100
H	7.836511	10.895214	6.334749
H	9.372064	10.607602	5.498992
H	7.851645	10.467555	4.611824
C	5.629932	8.680346	5.687483
H	5.284459	9.251298	6.556309
H	5.667699	9.349099	4.824135
H	4.890246	7.906336	5.471524
C	6.277323	5.682556	6.719646
H	6.055161	5.697682	7.791660
H	5.343989	5.827341	6.173599
H	6.659465	4.693970	6.457661
C	9.454445	5.436837	7.012112
H	9.585929	5.472101	8.098791
H	8.925375	4.515311	6.759727
H	10.444738	5.382168	6.552593
C	10.729819	8.292815	6.435015
H	10.977660	8.490524	7.483178
H	11.357352	7.463314	6.099289
H	11.000427	9.174840	5.850750
S	13.474314	3.622566	2.364013
Cl	7.712023	8.539599	2.628466
C	7.400526	5.417176	3.647138

DFT optimized xyz coordinates for C2m Cl up

Au	0.000000	0.000000	0.000000
Au	2.899130	0.000000	0.000000
Au	5.798270	0.000000	0.000000
Au	1.449570	2.510720	0.000000
Au	4.348700	2.510720	0.000000
Au	7.247830	2.510720	0.000000
Au	2.899130	5.021450	0.000000

Au	5.798270	5.021450	0.000000
Au	8.697400	5.021450	0.000000
Au	4.348700	7.532170	0.000000
Au	7.247830	7.532170	0.000000
Au	10.146970	7.532170	0.000000
Au	5.798270	10.042890	0.000000
Au	8.697400	10.042890	0.000000
Au	11.596530	10.042890	0.000000
Au	7.247830	12.553620	0.000000
Au	10.146970	12.553620	0.000000
Au	13.046100	12.553620	0.000000
Au	8.697400	0.000000	0.000000
Au	11.596530	0.000000	0.000000
Au	14.495670	0.000000	0.000000
Au	10.146970	2.510720	0.000000
Au	13.046100	2.510720	0.000000
Au	15.945230	2.510720	0.000000
Au	11.596530	5.021450	0.000000
Au	14.495670	5.021450	0.000000
Au	17.394800	5.021450	0.000000
Au	13.046100	7.532170	0.000000
Au	15.945230	7.532170	0.000000
Au	18.844370	7.532170	0.000000
Au	14.495670	10.042890	0.000000
Au	17.394800	10.042890	0.000000
Au	20.293930	10.042890	0.000000
Au	15.945230	12.553620	0.000000
Au	18.844370	12.553620	0.000000
N	10.004078	5.634202	3.791068
C	11.138225	6.334673	3.674008
C	11.175111	7.625685	3.177601
C	9.965709	8.253453	2.844466
C	8.788107	7.517843	2.976819
C	8.829940	6.191158	3.398788
C	7.044945	2.961779	3.672069
C	5.756740	3.287658	3.258456
C	5.418349	4.615361	2.981964
C	6.402153	5.597576	3.035968
C	7.705565	5.254112	3.399080
H	12.044420	5.833995	3.993544
H	12.119573	8.145715	3.067880
H	7.839763	7.981626	2.730209
H	7.259853	1.932838	3.941352
H	4.997783	2.512464	3.188736
H	4.393132	4.880398	2.743780

H	6.136469	6.627356	2.814185
Ir	9.793916	3.809236	4.835287
C	10.876341	2.744471	6.526407
C	11.851591	3.171776	5.605874
C	9.910683	1.900596	5.842056
C	11.515273	2.594719	4.318022
C	10.360696	1.754610	4.479677
C	10.815384	3.089736	7.978566
H	11.111100	2.218124	8.572847
H	11.484220	3.917839	8.218071
H	9.804976	3.387500	8.265017
C	8.787201	1.175759	6.516635
H	9.153309	0.290814	7.048838
H	8.287398	1.830974	7.233636
H	8.034973	0.850097	5.795084
C	9.797907	0.849666	3.428482
H	10.537011	0.096444	3.133905
H	8.908564	0.324639	3.782387
H	9.514890	1.410762	2.534943
C	12.368668	2.673609	3.102117
H	13.281668	2.078921	3.220418
H	11.815924	2.280692	2.248844
H	12.657765	3.701218	2.861399
C	13.046577	4.029091	5.895321
H	13.818477	3.458298	6.422279
H	13.497307	4.399910	4.970583
H	12.781618	4.891294	6.512614
S	9.952044	9.917953	2.260647
C	8.035945	3.942842	3.812092
Cl	8.666577	5.204214	6.476609

Reported densities of Ir piano-stool complexes

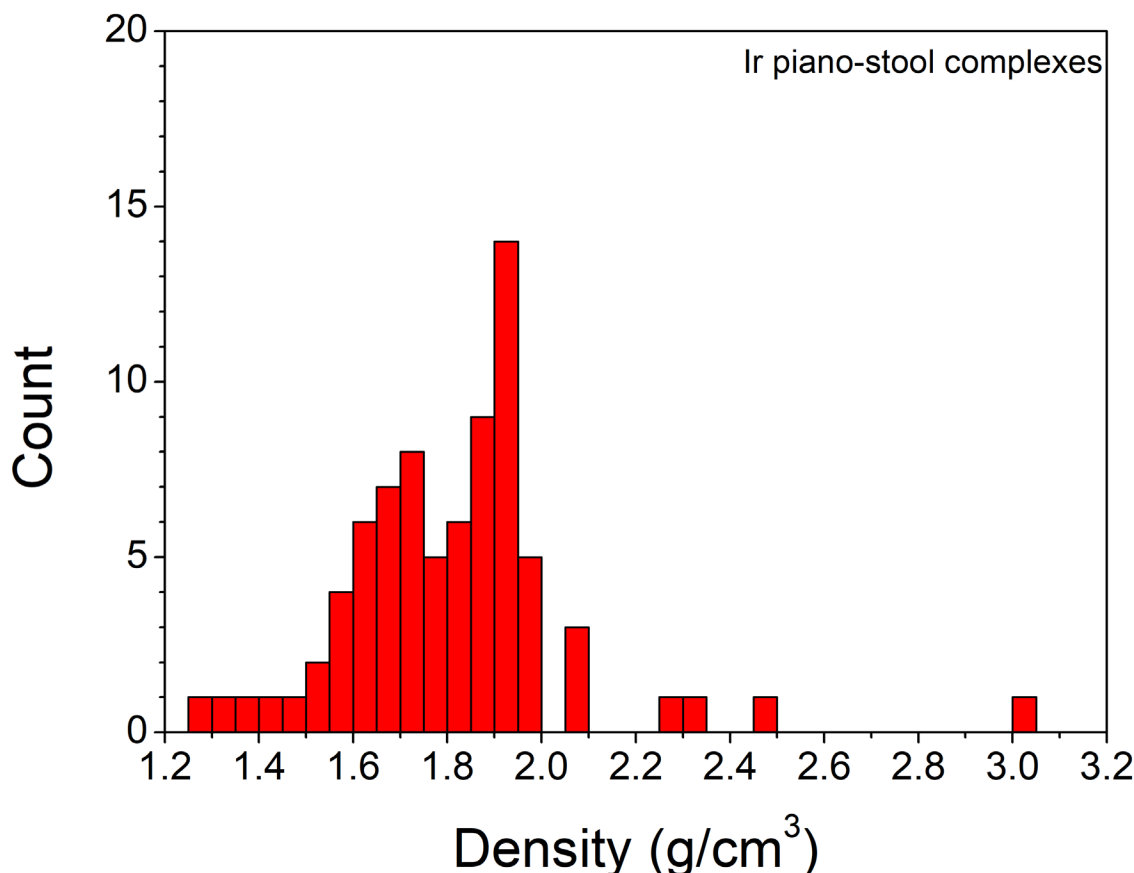


Figure S45. Histogram showing the reported density of Ir piano-stool complexes containing a halide and either a bipyridine or phenylpyridine moiety deposited in the Cambridge Structural Database³³ (78 structures).

References

1. M. Gliboff, L. Sang, K. M. Knesting, M. C. Schalnat, A. Mudalige, E. L. Ratcliff, H. Li, A. K. Sigdel, A. J. Giordano, J. J. Berry, D. Nordlund, G. T. Seidler, J.-L. Brédas, S. R. Marder, J. E. Pemberton and D. S. Ginger, *Langmuir*, 2013, **29**, 2166-2174.
2. D. L. Allara, A. Baca and C. A. Pryde, *Macromolecules*, 1978, **11**, 1215-1220.
3. D. L. Allara and R. G. Nuzzo, *Langmuir*, 1985, **1**, 52-66.
4. W. N. Hansen, *Journal of the Optical Society of America*, 1968, **58**, 380-390.
5. T. Buffeteau, B. Desbat and J. M. Turlet, *Appl. Spectrosc.*, 1991, **45**, 380-389.
6. J. D. E. McIntyre and D. E. Aspnes, *Surf. Sci.*, 1971, **24**, 417-434.
7. L. Sang, A. Mudalige, A. K. Sigdel, A. J. Giordano, S. R. Marder, J. J. Berry and J. E. Pemberton, *Langmuir*, 2015, **31**, 5603-5613.
8. H. Wang, PhD Thesis, The University of Arizona., 2011.
9. J. Wang, M. L. Clark, Y. Li, C. L. Kaslan, C. P. Kubiak and W. Xiong, *J. Phys. Chem. Lett.*, 2015, **6**, 4204-4209.
10. D. A. Sheik, J. M. Chamberlain, L. Brooks, M. Clark, Y. H. Kim, G. Leriche, C. P. Kubiak, S. Dewhurst and J. Yang, *Langmuir*, 2017, **33**, 2596-2602.
11. C. Baker, I. P. Cockerill, J. E. Kelsey and W. F. Maddams, *Spectrochimica Acta Part A: Molecular Spectroscopy*, 1978, **34**, 673-682.
12. C. Baker, P. S. Johnson and W. F. Maddams, *Spectrochimica Acta Part A: Molecular Spectroscopy*, 1978, **34**, 683-691.

13. P. K. Mallick, G. D. Danzer, D. P. Strommen and J. R. Kincaid, *The Journal of Physical Chemistry*, 1988, **92**, 5628-5634.
14. P. A. Vekariya, P. S. Karia, J. V. Vaghasiya, S. Soni, E. Suresh and M. N. Patel, *Polyhedron*, 2016, **110**, 73-84.
15. P. Štarha, Z. Dvořák and Z. Trávníček, *J. Organomet. Chem.*, 2018, **872**, 114-122.
16. H.-D. Amberger and H. Reddmann, *J. Organomet. Chem.*, 2010, **695**, 2455-2460.
17. É. Bencze, B. V. Lokshin, J. Mink, W. A. Herrmann and F. E. Kühn, *J. Organomet. Chem.*, 2001, **627**, 55-66.
18. K. L. Materna, B. Rudshteyn, B. J. Brennan, M. H. Kane, A. J. Bloomfield, D. L. Huang, D. Y. Shopov, V. S. Batista, R. H. Crabtree and G. W. Brudvig, *ACS Catal.*, 2016, **6**, 5371-5377.
19. S. Bayari, A. Topaçlı and A. Aydinli, *Spectrosc. Lett.*, 1994, **27**, 1083-1096.
20. J.-D. Chai and M. Head-Gordon, *PCCP*, 2008, **10**, 6615-6620.
21. J. P. Perdew, K. Burke and M. Ernzerhof, *Phys. Rev. Lett.*, 1996, **77**, 3865-3868.
22. S. Grimme, S. Ehrlich and L. Goerigk, *J. Comput. Chem.*, 2011, **32**, 1456-1465.
23. K. P. Kepp, *The Journal of Physical Chemistry A*, 2017, **121**, 2022-2034.
24. W. J. Hehre, R. Ditchfield and J. A. Pople, *J. Chem. Phys.*, 1972, **56**, 2257-2261.
25. P. C. Hariharan and J. A. Pople, *Theor. Chim. Acta*, 1973, **28**, 213-222.
26. M. M. Franci, W. J. Pietro, W. J. Hehre, J. S. Binkley, M. S. Gordon, D. J. DeFrees and J. A. Pople, *J. Chem. Phys.*, 1982, **77**, 3654-3665.
27. P. J. Hay and W. R. Wadt, *J. Chem. Phys.*, 1985, **82**, 299-310.
28. F. Weigend, *PCCP*, 2006, **8**, 1057-1065.
29. F. Petersen, I. Lautenschläger, A. Schlimm, B. M. Flöser, H. Jacob, R. Amirbeigiarab, T. R. Rusch, T. Strunkus, O. Magnussen and F. Tuczek, *Dalton Trans.*, 2021, **50**, 1042-1052.
30. Y. S. Chi, S. Hwang, B. S. Lee, J. Kwak, I. S. Choi and S.-g. Lee, *Langmuir*, 2005, **21**, 4268-4271.
31. G. Valincius, G. Niaura, B. Kazakevičienė, Z. Talaikytė, M. Kažemėkaitė, E. Butkus and V. Razumas, *Langmuir*, 2004, **20**, 6631-6638.
32. O. Reynes, C. Bucher, J.-C. Moutet, G. Royal and E. Saint-Aman, *Inorg. Chim. Acta*, 2008, **361**, 1784-1788.
33. C. R. Groom, I. J. Bruno, M. P. Lightfoot and S. C. Ward, *Acta Crystallographica Section B*, 2016, **72**, 171-179.